
3D-Printed Whisker Transducer

Authors:
John Delamare

Supervisors:
prof.dr.ir. G.J.M. Krijnen
ing. R.G.P. Sanders

Abstract

Whiskers are specialized hairs which some mammals such as sea lions, cats, rats etc. use to sense stimuli from their surrounding environment. In this project we will investigate whether such a whisker transducer can be fabricated using a 3D printer. Furthermore the device is to operate on the principle of capacitive sensing. As the methods from printing conductive materials are limited, the capacitance will be induced by interaction between a PCB and the printed whisker. The objective of the device is to be able to measure the point of contact force along the whisker. To do this the device should be able to measure 2-DOF and decouple the forces acting on the whisker in order to determine the contact location.

Contents

1	Introduction	5
1.1	Whisker	5
1.2	3D Printing	6
1.3	Previous Work	6
1.3.1	Piezo	6
1.3.2	Hall-effect	7
1.3.3	Capacitive	7
1.3.4	Our Approach	8
1.4	Discussion	8
1.5	Conclusion	8
2	Modeling	10
2.1	Mechanics	10
2.2	Transduction	11
2.2.1	Capacitance calculation	12
2.3	Proposed Model	20
2.3.1	Structure	20
2.3.2	PCB Patterns	23
2.3.3	Discussion	27
2.3.4	Conclusion	27
3	Fabrication	28
3.1	Structure	28
3.1.1	Objet	28
3.1.2	Ultimaker	28
3.1.3	Print Orientation	28
3.2	Discussion	29
3.3	Conclusion	29
4	Measurement and Results	30
4.1	Validation Method	30
4.2	Mechanical Dynamics	31
4.2.1	Rotation and Translation	31
4.2.2	Hysteresis	32
4.2.3	Creep	33
4.3	Capacitance	34
4.4	Complete Prototype	34
4.5	Conclusion	34
5	Discussion	35
6	Conclusion	35
6.1	Recommendation	36
	References	37
	Appendix A Capacitance Calculations	40
A.1	Volume intagrals	40

Appendix B Model	42
Appendix C PCB Layout	43
Appendix D 3D Prints	44
Appendix E Matlab Code	45
Appendix F Openscad Code	54

1 Introduction

1.1 Whisker

Humans primarily rely on their skin and fingertips for tactile sensation. However many other mammals both land and aquatic rely on whiskers (vibrissae) in order to sense the environment around them. Whiskers are hairs with a specialized structure and mechanical properties. Each species uses them for different functions. Harbour seals are able to detect hydrodynamic stimuli left behind by their prey in turbid waters [1]. Rats are able to use their whiskers during exploration to extract information from objects in their near environment. They are able to determine various object features such as size, shape, texture, orientation, and location [2]. Around the base of the whisker shaft there are hundreds of neuro-receptors, these detect the deflection of the whisker much like an old record player detects the bumps and dips on a record [3]. As such tactile sensing using whisker offers several benefits, such as being able to discern objects and the surrounds in an unlit environment. Moreover objects can be mapped without having to come in direct contact with the skin(receptors), which may be damaged due to direct contact depending on the properties of the object surface, imagine hot objects. Studies suggest that the receptors at the base of the whisker encode information about the base torques, velocities, and duration of the whisker displacement [3]. Using this encoded information they are able to implicitly estimate the contact location along the whisker [4]. There are multiple whiskers on a rats face that are arranged in a grid of 5 rows having up to 9 whiskers each [3, 5], see Fig. 1.1, increasing in length from the front of the rat to the back reaching up to 50 mm and diameters tapering from 1 mm [3]. Many studies on the mechanical and structural properties of the whisker suggest that properties such as dimensions, curvature, elasticity, resonance, and damping play critical roles on the the signal measured at the base of the structure [3]. The rats whisker is not a passive sensor waiting to come into contact with objects in the environment. The whiskers are actively protracted and retracted in a rhythmic movement at around 5 Hz-25 Hz [5]. Each whisker is able to be controlled individually which allows the rat a greater capability to effectively sense its surroundings [3].



Figure 1.1: Rat with whisker.

1.2 3D Printing

Additive manufacturing, also known as 3D printing, is a process in which material is added together layer by layer to build an object. The layer thickness are typically a few hundred microns, however depending on the type of printer better resolutions can be achieved. 3D printers use models created in graphical design programs, from which it generates 2 dimensional horizontal slices which are then printed on top of each other. This method of printing allows for the printing of very complex designs which would otherwise be costly or time consuming using other manufacturing methods. This makes 3D printing ideal for prototyping of designs structures, though small scale manufacturing is also possible. However with designing complex structures, which for example have any horizontal overhang, support structures are usually needed to hold the material in place. There are several ways of 3D printing, each depositing material in a different method which leads to different attainable resolutions. Moreover different materials are used for 3D printing, from plastics to metals. It is also possible to print multiple materials on one structure within one printing session. This however is very challenging as there are many variables which will affect the final print quality such as adhesion, surface energy, print temperature, and processing conditions among others [6]. And these challenges would vary for each type of printer.

1.3 Previous Work

There have been various implementations of a whisker transducer which function as tactile or fluid flow sensors, each implementation using various different materials ranging from steel to an actual rat whisker [3]. Moreover there have been a variety of transduction methods which aim to simulate the function of the whisker base such as potentiometers, capacitors, hall-effect sensors, strain gauges [3], each method having certain advantages and certain shortcomings. In this section we will describe some of the previous implementations and outline our approach. Each implementation is primarily characterized by the transduction method.

1.3.1 Piezo

Piezo-electric

F. Ju *et al.* [7] designed a micro whisker transducer with a single degree of freedom which could simultaneously measure mechanical impedance and actuate the whisker to simulate whisking. This was done using a piezo-electric bimorph with a steel whisker attached to it. A bimorph is a structure consisting of two layers dissimilar electrical, or thermal properties. The piezo-electric bimorph reacts asymmetrically when a potential is applied to the layers, thus when one layer contracts the other expands. Due to it being made of piezo-electric material the material changes its charge concentration under the influence of mechanical stress. With these two properties the authors of [7] are able to derive a transduction matrix which shows the relationship between induced moments on the whisker and the actuation it undergoes.

Piezo-resistive

Piezo-resistive elements are similar in some ways to piezo-electric, however they are only able to change their electrical conductivity when mechanical stress is applied to the structure. In [8] the authors propose two implementations with this measuring principle which measure 2 degrees of freedom. The designs is able to bend in two orthogonal directions In the first design the whisker is supported on a cross which allows it limited rotation in two directions, with strain-gauges placed on the cross to measure the strain caused when bending. The second implementation places the strain gauges directly on the whisker.

1.3.2 Hall-effect

The Hall-effect sensor produces a voltage when exposed to a magnetic field. By varying the magnetic field the voltage then also varies. In [9] the authors connect a magnet to the base of a whisker, which is then placed on top of a Hall-effect sensor. As forces are applied to the whisker it is able to rotate about its pivot point causing the magnet to move and vary the induced magnetic field on the sensor.

1.3.3 Capacitive

Capacitance is formed by opposing charge build-up on separate electrodes. The basic equation for a capacitor is $Q = CV$, which relates the capacitance to the charge accumulated on the surface of a set of electrodes, and the voltage potential between the electrodes. From a given voltage potential we can find the work required to transfer charge from one electrode to the other by [10]

$$V = \frac{Q}{C} \quad (1)$$

$$dU = V dQ \quad (2)$$

Then integrating from zero charge

$$U = \int_0^Q \frac{Q'}{C} dQ' \quad (3)$$

$$U = \frac{1}{2} \frac{Q^2}{C} \quad (4)$$

There are different implementations of a capacitive whisker sensor, however they are used primarily for flow sensing. One such model is described by N. Izadi in [11], shown in Fig. 1.2. The design makes use of a parallel plate capacitor geometry, for which the capacitance resolves to being approximated by $C = \frac{\epsilon_0 \epsilon_r A}{d}$ Where A = area, ϵ_0, ϵ_r = relative permittivity of vacuum and the desired material respectively, and d = distance between plates. One can easily see that by changing the area or the distance between the plates the capacitance can be affected which can then be measured using additional electronics. Though the design is developed as a flow-sensor, with modification, it would be able to be adapted as a tactile sensor. In the design the whisker base is supported on a membrane which deforms according to the deflection of the whisker structure, caused by the flow along it.

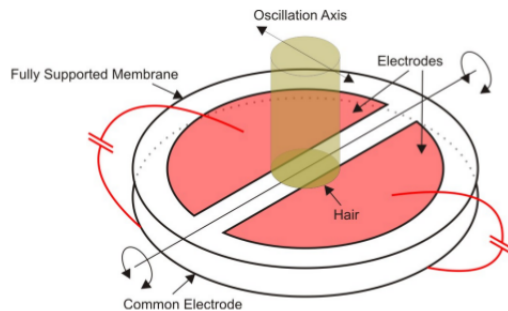


Figure 1.2: Flow sensing whisker design [14].

Attached to the bottom of the membrane are two planar electrodes oriented perpendicular to the direction of motion of the whisker. These two electrodes are used to measure differential capacitance in order to determine the moment on the structure. Though the implementation is done on a MEMS level, there are also other implementations which are much larger such as those found in [12,13].

1.3.4 Our Approach

In this project we attempt to design a 3D printed passive whisker sensor, that is, without active whisking capability. This model will be placed on a patterned printed circuit board (PCB) and make use of the fringing fields of the capacitance to be able to measure the movement of the whisker base. The proposed model should have 2 degrees of freedom and fabricated using a 3D-printer. Focus is placed on making a design that can be printed and attached to a small PCB board and could possibly be applied to environment mapping for robots. As such a minimal number of components is desired in the design. Different materials and 3D printers will be considered in the process, considering applicability and availability. An advantage of this approach is the reduced difficulty and production time in developing a modular tactile sensor.

1.4 Discussion

The implementations shown in this section give a general overview of the approaches which have been used to design a whisker sensor. From the implementations discussed only one had 2 degrees of freedom, however these were perpendicular to each-other. Thus the model is able to bend in orthogonal directions, and is only able to measure the bending on those directions, and not contact location. The models which are able to detect contact location make use of active whisking, by use of actuators such as a motor, or a bimorph in one case. Moreover the transduction methods varied from resistive to capacitive.

1.5 Conclusion

No implementations were found which were implemented fully using a 3D-printer. Moreover, current implementation do not make use of 2 degrees of

freedom, but rely on additional actuation to determine contact location. Furthermore there have been no known sensor implementations which try to exploit the inherent capacitance of a printed circuit board.

2 Modeling

2.1 Mechanics

In this section we will investigate the forces and moments acting on the whisker which are implicitly sensed by the rat in order to generate a model on which we will base the sensor. The base of the whisker is more accurately modeled as a torsional spring in the event of initial object contact and boundary whisking [15]. With this taken into consideration a free-body diagram of the system is shown in Fig. 2.1. From the figure a set of equilibrium equations can be derived where

$$\begin{aligned}\Sigma F_x &= 0 \\ \Sigma F_y &= 0 \\ \Sigma \tau &= 0\end{aligned}$$

In the case where there is no force acting on the whisker (5).

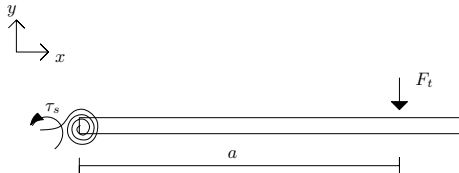


Figure 2.1: Whisker Free-body Diagram.

$$\Sigma \tau = \tau_s + \tau_d = 0 \quad (5)$$

$$\begin{aligned}\tau_s &= -k_r \theta \\ \tau_d &= -b_r \dot{\theta}\end{aligned}$$

Where τ denotes the torque caused on the structure. The subscripts s and d denote the components for the spring and drag components respectively. And θ the angle of rotation. This leads to the homogeneous differential equation for the torque (6). Where k_r is the torsional spring constant, b_r the damping ratio, and J the moment of inertia of the beam.

$$J\ddot{\theta} + b_r \dot{\theta} + k_r \theta = 0 \quad (6)$$

When there is a force acting on the whisker as in Fig. 2.1, then (6) becomes (7).

$$J\ddot{\theta} + b_r \dot{\theta} + k_r \theta = F_t a \quad (7)$$

Thus being able to measure the angle θ would allow determination of the torque caused by the contact force. However this is not sufficient to determine the precise contact location. In order to do this a second equation is needed. The introduction of a second degree of freedom allows the formulation of another equation which describes the motion in said degree.

This motion will also be dependent on the force acting on the whisker. If this motion is only dependent on the force and not the contact location it will allow

Radius (μm)	E (GPa)	k(Nmm/rad)	b (Nmm/s/rad)
91.4	4.5	$65.3 \cdot 10^3$	$0.141 \cdot 10^3$

Table 2.1: Mechanical properties at whisker base. [4]

us to set up a system of 2 equations, and 2 unknowns F_t & a . The new model is shown in Fig. 2.2. From which the second equilibrium equation follows (8). The rest of the equation is derived similar to Eq. (5)-(7).

$$\Sigma F_y = F_s + F_d = 0 \quad (8)$$

$$F_s = k_t y$$

$$F_d = b_t \dot{y}$$

This leads to a new system of equations for our structure, (10) and (9). By

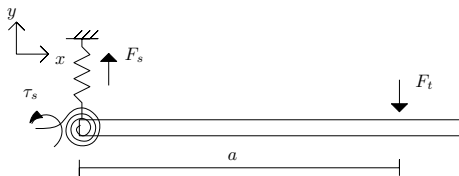


Figure 2.2: Design Model.

simultaneously solving these two equations we should be able to determine the value of a .

$$m\ddot{y} + b_t\dot{y} + k_t y = F_t \quad (9)$$

$$J\ddot{\theta} + b_r\dot{\theta} + k_r\theta = F_t a \quad (10)$$

In [4] the authors investigate the dynamic model of a rat whisker for situation of contact and non-contact whisking. By observing the frequency response of a rat whisker, they were able to develop a model which would match the response. From the model they were then able to derive the mechanical properties of the whisker. The results show that the mechanical characteristics of the whisker vary along the whisker. Moreover, evidence suggest that the rats may actively modulate the bio-mechanical parameters of the whisker which could affect damping. The parameters at the base of the whisker [4] are shown in Tab. 2.1. It should also be noted that a whisker is not a rigid body as one can see from the given Young's modulus. This means that the whisker experiences bending moments when a force is exerted on it. However for the purpose of this design the bending effect will not be taken into consideration. Our model will focus on the equilibrium conditions, thus all bending moments will be felt at the base.

2.2 Transduction

The proposed design is intended to make use of the inherent capacitance induced by printed circuit board (PCB) electrodes. Due to the lack of the capability

to print conductive materials the design must allow for a dielectric material to interact with the electric field generated by the PCB electrodes to make a change to the total capacitance. A rotation in the mechanical domain will result in a reduction of the gap between the conductor and the dielectric as shown in Fig. 2.3.

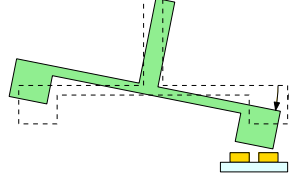


Figure 2.3: Whisker Rotation.

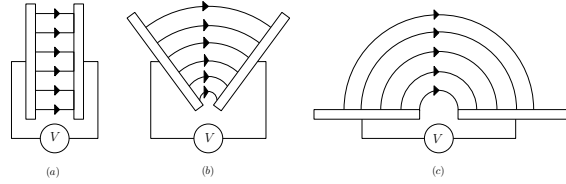


Figure 2.4: Transformation standard capacitor.

In this configuration we have a co-planar capacitor which can be imagined as the transformation of a standard capacitor as shown in Fig. 2.4(c) When the gap between the whisker base and the conductor is sufficiently small the electric field between them be approximated as a continuous distribution of semi-circles.

2.2.1 Capacitance calculation

Method 1: Volume Integration

Different methods of calculating the capacitance were attempted which will be outlined and compared in this section. The capacitance and voltage are related to the co-energy function by Eq. (11), from which Eq. (12) follows. The total free energy can be calculated from Eq. (13) [16].

$$U = \frac{1}{2}CV^2 \quad (11)$$

$$\Rightarrow C = \frac{2U}{V^2} \quad (12)$$

$$U = \frac{\epsilon}{2} \int_V \mathbf{E}^2 dV \quad (13)$$

Using the semi-circle approximation within the given range, it can be seen that the electric field is uniform from one conductor to another reducing in magnitude

as the radius of the semi-circles increases. If a known potential is placed across the conductors then the electric field can be found using (15).

$$\int_a^b \mathbf{E} \cdot d\vec{s} = -\Delta\Phi \quad (14)$$

$$E \cdot \pi r = -\Delta\Phi$$

$$\Rightarrow E = \frac{-\Delta\Phi}{\pi r} \quad (15)$$

With the known electric field the energy can be calculated in the desired volume. The integration intervals are determined by the coordinate system used along with Fig. 2.5. No dimensions are given in order to allow optimization of the model. Using cylindrical coordinates the r is made to vary as a function of θ in order to set the desired boundaries. Furthermore the boundary conditions in Eq. (16) and (17) must be met for continuity of the field. Where D is the displacement field in the dielectric material defined as (18).

$$E_{below}^{\parallel} = E_{above}^{\parallel} \quad (16)$$

$$D_{below}^{\perp} = D_{above}^{\perp} \quad (17)$$

$$\vec{D} = \epsilon\vec{E} \quad (18)$$

Nevertheless this method leads to a set of rather complicated integrals which are not practical to work with and also provide results which are rather complex. Further elaboration on the calculation is given in Appendix A.

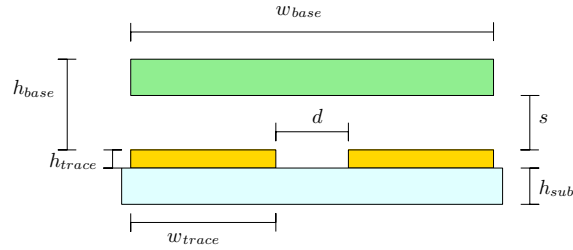


Figure 2.5: Dimensions

Method 2: Asymptote

In this method we use the two extremes of the gap between the dielectric and electrodes. The assumption of a uniform field of semi-circles is used again, under the two different conditions. In the first situation, the energy is calculated when the dielectric whisker base is completely absent. In the second situation the capacitance is calculated with the dielectric directly sitting on the electrodes as shown in Fig. 2.6a

This leads to energy Eq. (19), (20), and (21) for air, dielectric, and the substrate

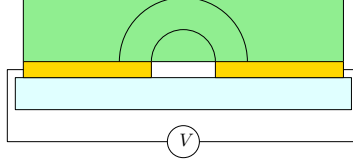


Figure 2.6a: Co-planar capacitor with dielectric layer.

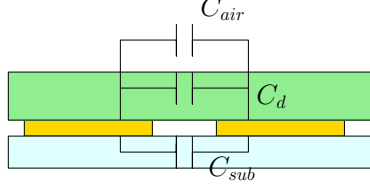


Figure 2.6b: Capacitance connection.

respectively.

$$U_{\text{air}} = \frac{\epsilon_0 \Delta\Phi^2 L}{2\pi} \ln\left(\frac{2w_{\text{trace}}}{d}\right) \quad (19)$$

$$U_{\text{die}} = \frac{\epsilon_0 \epsilon_d \Delta\Phi^2 L}{2\pi} \ln\left(\frac{2w_{\text{trace}}}{d}\right) \quad (20)$$

$$U_{\text{sub}} = \frac{\epsilon_0 \epsilon_s \Delta\Phi^2 L}{2\pi} \ln\left(\frac{2w_{\text{trace}}}{d}\right) \quad (21)$$

L : trace length perpendicular to page

Using the voltage potential and (12) we can then derive the two asymptotes of the system which are then given by (22) and (23). Since the substrate is always present, its capacitance is added to both equations.

$$C_{\text{air}} = \frac{\epsilon_0 (1 + \epsilon_s) L}{2\pi} \ln\left(\frac{2w_{\text{trace}}}{d}\right) \quad (22)$$

$$C_{\text{die}} = \frac{\epsilon_0 (\epsilon_d + \epsilon_s) L}{2\pi} \ln\left(\frac{2w_{\text{trace}}}{d}\right) \quad (23)$$

The whisker base 'capacitance' is connected at the same points as the substrate 'capacitance' thus the two are parallel to each other as shown in Fig. 2.6b. In Fig. 2.7 the capacitance, with the whisker base sitting directly on the traces, is plotted as a function of the trace width and gap between the traces. The capacitance will increase as the the width of the traces increases. This reduces more of the non-linear effects caused at the edges of the capacitor effectively increasing the area. Similar to what we would expect to happen in Fig. 2.4(a) if the electrodes were made wider or longer. This effect is in agreement with findings in [17], which showed that the impedance would drop as a function of $\frac{w_{\text{trace}}}{d}$.

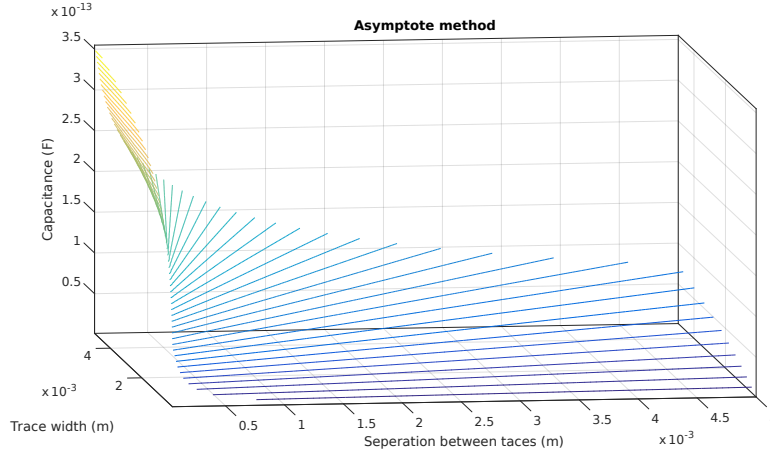


Figure 2.7: Capacitance vs Trace width (w_{trace}) and the gap (d)

Method 3: Conformal Mapping

The Schwarz-Cristoffel Transformation (SCT) is a conformal mapping technique to map a point on the complex z -plane to a point on the complex w -plane. A polygon in the z -plane is transformed to a line on the real axis in the w -plane, with the interior of the polygon mapped to the upper half of the plane and vice versa [18], see Fig. 2.8.

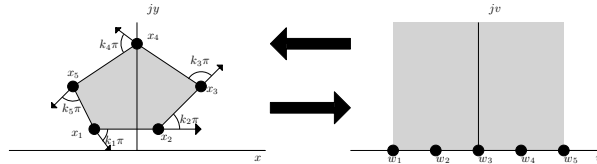


Figure 2.8: Schwarz-Cristoffel Transformation

$$z = x + jy$$

$$w = f(z) = u(x, y) + jv(x, y)$$

$$\frac{\partial u}{\partial x} = \frac{\partial v}{\partial y} \quad (24)$$

$$\frac{\partial u}{\partial y} = -\frac{\partial v}{\partial x} \quad (25)$$

In order for a function to be conformal it must meet the Cauchy-Riemann condition (24) and (25). This means that the planes are orthogonal and will preserve

angles between curves in the planes through transformation [19]. The orthogonality of the planes leads to some useful properties listed below [20].

- Laplace's equation remains invariant through transformation
- The geometrical shape of the configuration is changed, without any change in the electrostatic energy thus no change in the capacitance either.
- The physical boundaries remain unchanged

It must be noted however that the solutions using the SCT method are valid only for static or quasi static cases [20]. The transformation between domains is given by Eq. (26), where A determines the size and orientation of the polygon and B determines the position thereof.

$$w = f(z) = A \int_{z_0}^z (z' - x_1)^{-k_1} (z' - x_2)^{-k_2} \dots (z' - x_{n-1})^{-k_n} dz' + B \quad (26)$$

$$k_1 + k_2 + k_3 + \dots + k_n = 2$$

There also exists an inverse SCT which is defined by $z = f^{-1}(w)$. The function which maps the boundary of a rectangle in the z -plane to a line on the real axis w -plane is the elliptic sine function (ESF), where the inverse ESF, also termed complete elliptical integral of the first kind [21], is defined as Eq. (27) and (28). k is called the elliptic modules and k' is its complimentary.

$$K(k) = \int_0^1 \frac{dz}{\sqrt{(1-z^2)(1-k^2z^2)}} \quad (27)$$

$$\text{for } 0 \leq z \leq 1$$

$$K(k) + jK'(k) = \int_0^1 \frac{dz}{\sqrt{(1-z^2)(1-k^2z^2)}} + \int_0^{\frac{1}{k}} \frac{dz}{\sqrt{(1-z^2)(1-k^2z^2)}} \quad (28)$$

$$\text{for } 0 \leq z \leq \frac{1}{k}$$

$$K'(k) = K(k')$$

$$k' = \sqrt{1-k^2}$$

When working with parallel planar transmission lines the characteristic impedance is defined by (31). The ratio $\frac{K(k)}{K(k')}$ can be approximated by (29) which has a relative error which is less than 4×10^{-12} [21].

$$\frac{K(k)}{K(k')} \approx \frac{\pi}{\ln 2 \frac{1+\sqrt{k'}}{1-\sqrt{k'}}}, \text{ for } 0 \leq k \leq \frac{1}{\sqrt{2}} \quad (29)$$

$$\frac{K(k)}{K(k')} \approx \frac{\ln 2 \frac{1+\sqrt{k}}{1-\sqrt{k}}}{\pi}, \text{ for } \frac{1}{\sqrt{2}} \leq k \leq 1 \quad (30)$$

$$Z_0 = \frac{\eta}{4} \frac{K(k)}{K(k')} \quad (31)$$

$$\eta = \sqrt{\frac{\mu}{\epsilon}}$$

If the impedance is purely reactive then we know that the capacitance C is inversely proportional to the impedance [10]. However this provides some conflict between Eq. (31) from [21] and [22], [20], [23] among others which suggest that C is proportional to $\frac{K(k)}{K(k')}$. Nevertheless the capacitance can be calculated from Z_0 by use of Eq. (32) [24]. Note that this is the capacitance per unit length.

$$\begin{aligned} \frac{C_0}{\sqrt{\epsilon\mu}} &= \frac{1}{Z_0} \\ \Rightarrow C_0 &= \frac{\sqrt{\epsilon\mu}}{Z_0} \end{aligned} \quad (32)$$

The elliptic modulus k can be computed in terms of Jacobi theta function of zero argument and nome q [25] as show in Eq. (33) and (34).

$$k = \frac{\vartheta_2^2(0, q)}{\vartheta_3^2(0, q)} \quad (33)$$

$$\begin{aligned} q &= e^{i\pi\tau} \\ &= e^{-\pi \frac{K(k')}{K(k)}} \end{aligned} \quad (34)$$

There are other methods of calculating the elliptical modulus k such as first transforming to the intermediate t -plane and then to the w -plane [18,20,26–28]. However the exact process is not discussed in this paper. Other authors have calculated k directly with the use of hyperbolic trigonometric functions [20,23,29,30]. In [30], the authors suggest that Eq. (35) is used for configurations which have a ground plate backing, and Eq. (36) when no ground plate is present. Where h_i is the height of a given layer, and as $h \rightarrow \infty$, $k_0 \approx \frac{2}{w_{trace} + 2d}$ [23]. The k_0 modulus is for the calculation of the characteristic capacitance, $h \rightarrow \infty$ as there are no additional layers which means the surrounding medium has infinite thickness.

$$k_i = \frac{\tanh \frac{\pi w_{trace}}{4h_i}}{\tanh \frac{\pi(\frac{w_{trace}}{2} + d)}{2h_i}} \quad (35)$$

$$k_i = \frac{\sinh \frac{\pi w_{trace}}{4h_i}}{\sinh \frac{\pi(\frac{w_{trace}}{2} + d)}{2h_i}} \quad (36)$$

$$i = 1, 2, \dots$$

Combining (36), (32) and (29) the capacitance of the different layers can be calculated in order to determine the total capacitance.

For cases which the relative permittivity ϵ_r decreases monotonically across the layers the capacitors should be connected in parallel (37), and when the relative

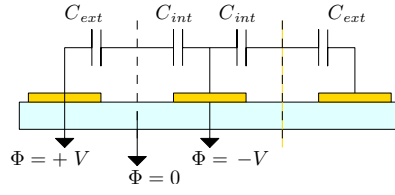


Figure 2.9: Capacitor cell.

permittivity increasing across the layers, the capacitors should be connected in series (38) [31].

$$C_{\text{cell}} = L \left[\sum_{i=1}^{n-1} (\epsilon_{r,i} - \epsilon_{r,i+1}) C_i + \epsilon_{r,n} C_n \right] \quad (37)$$

$$\frac{1}{C_{\text{cell}}} = \frac{1}{L} \left[\sum_{i=1}^{n-1} \left(\frac{1}{\epsilon_{r,i}} - \frac{1}{\epsilon_{r,i+1}} \right) \frac{1}{C_i} + \frac{1}{\epsilon_{r,n}} \frac{1}{C_n} \right] \quad (38)$$

C_{cell} is defined as one pair of exterior (C_{ext}) and interior (C_{int}) capacitance as shown in Fig. 2.9. The figure also shows the equipotential boundaries between the electrodes. The resulting capacitance for a single cell as a function of w_{trace} and d is plotted in Fig. 2.10.

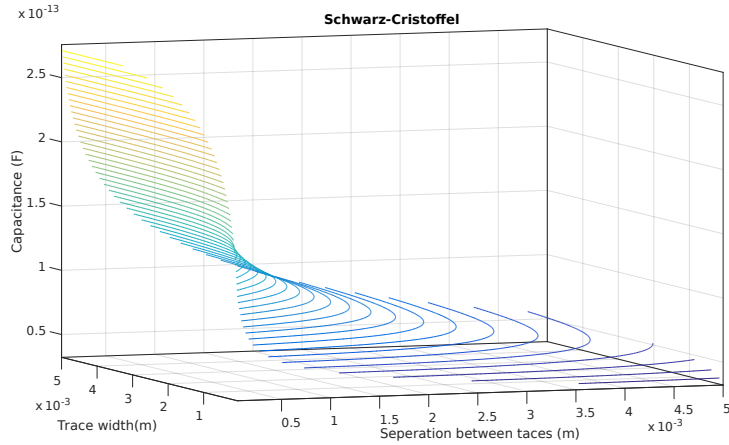


Figure 2.10: SCT Capacitance vs w_{trace} and d .

Discussion of Methods

The two capacitance plots were made using the parameters in Tab. 2.2, with the dielectric directly on the electrodes, i.e. $s = 0$. This was done with a fixed length. The two surfaces show some similarity however the *Asymptote method* shows an increasing slope with increasing trace width between the electrodes with larger separation. Both plots show an increase of capacitance with an increase of trace width, which would increase the effective area of the capacitor. The ratio of the capacitance for the two methods $\frac{C_{SCT}}{C_{as}}$ was investigated and is plotted in Fig. 2.11. We see from this figure that the relative difference is constant for trace separation, however for trace width the relative difference reduces with increasing trace width. As the trace widths increase it is assumed that the approximation of the *Asymptote* method would improve the semi-circle approximation, as non-linearities in the electric field would be reduced.

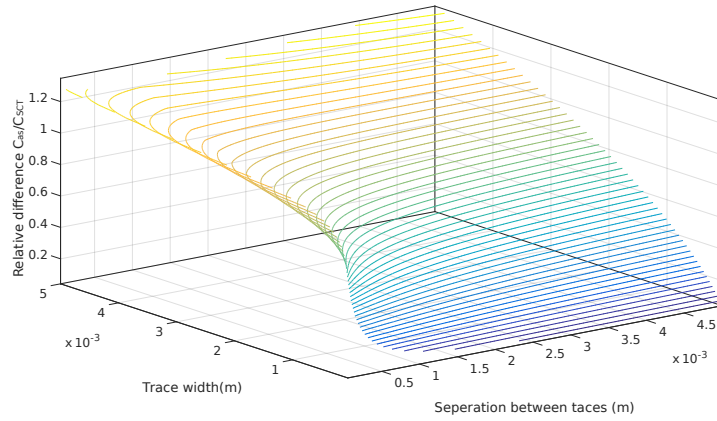


Figure 2.11: Relative difference between capacitance methods.

Analyzing Fig 2.11 with this assumption, we can make an interpretation of the accuracy of the *SCT* method used. As the width increase and the *Asymptote* approximation increases in accuracy it also tends to the *SCT* approximation reaching a ratio of 1 at a width of approximately 3.5 mm. This equality line would give a possibility of experimentally measuring and comparing the effectiveness of each method.

ϵ_0	8.854×10^{-12}
ϵ_d	2.3
ϵ_{sub}	5

Table 2.2: Tab. of Relative permittivities.

2.3 Proposed Model

2.3.1 Structure

Recall Eq. (10) and (9) describe the desired behavior of the whisker. Furthermore in order to increase the responsiveness of the system it should be critically damped [32]. Another factor which influences the responsiveness of the system is the distance between the rotating arm upon which the torque is acting and the capacitor area [14]. Take Fig. 2.3 as an example, if the electrodes were further out from the center, there would be a much larger displacement for a smaller angle. The base structure chosen for this prototype is shown in 2.12 with the dimensions given in Appendix B Fig. B.1.

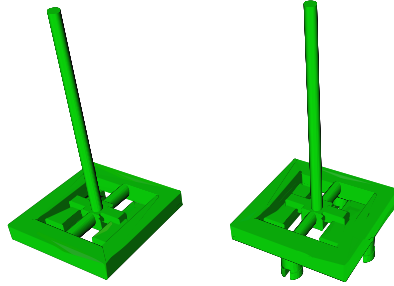


Figure 2.12: Model Structure.

The structure chosen supports the whisker base by connecting it on both sides with elliptical bars. This structure would allow for both rotation and lateral displacement of the whisker base, which would be determined primarily by the beams length, cross-section, and the material properties. As a force acts on the whisker the induced torque would cause the base to rotate, causing torsion on the cross-section of the elliptical bars as shown in Fig. 2.13a. The angular twist on an elliptical cross-section is defined by Eq. (39) [33].

$$\theta = \frac{\tau L}{JG} \quad (39)$$

$$J = \frac{\pi a^3 b^3}{a^2 + b^2}$$

$$a = \frac{h_s}{2}, \quad b = \frac{w_s}{2}$$

G : Modulus of rigidity

The support structure acts like a beam fixed at both ends. When a force acts on the center of the beam, i.e. the whisker base, the beam should deflect in

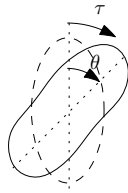


Figure 2.13a: Torsion on elliptical cross-section.

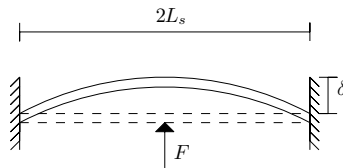


Figure 2.13b: Fixed beam deflection.

the same direction as the force. The deflection is given by (40), which is the deflection of a cantilever fixed cantilever beam reduced by a factor of 2. This reduction is due to the assumption that the structure is two cantilever beams connected at the center, with the force being equally distributed between them, when in equilibrium. Thus the force is reduced by a factor of 2, due to the two beams. Therefore the deflection of a single cantilever beam will also be reduced by a factor of 2.

$$\delta = \frac{FL_s^3}{6EI} \quad (40)$$

E : Young's Modulus

I : Area moment of inertia

The dimensions of the support structure were optimized for maximum displacement in 2 domains, however there is a trade-off between maximizing displacement and maximizing rotation. This is because both the twist angle and the deflection are related to the cross-section of the beam through variables I & J . The deflection can be optimized using the length of the support beams. However there is a practical limit to how long the support beams should be made, as we are trying to design a sensor. Dimensions more optimal for displacement lead to quicker rupture in the rotational domain. From Fig. 2.12 one can also notice the large pads on both sides of the whisker base which will be used as the dielectric surface area for the capacitance. With a larger dielectric surface area a larger change in the overall capacitance is expected.

Material

The rotation and deflection are dependent on the modulus or rigidity and the Young's modulus, which are not dependent on the geometry of an object but on its material properties. The lower the value of G the easier the structure will be allowed to rotate, same counts for the deflection *w.r.t.* E . As the structure is to be 3D-printed, the choice of material is limited.

E	3.5 GPa
G	2.4 GPa
Elongation at break	6 %

Table 2.3: PLA Properties [34].

Moreover the choice of 3D-printer also limits the range of materials available for use. Furthermore the availability of data on the properties of 3D-printed material is limited and sometimes differing between sources. For this prototype *PLA* was used to print the structure, the material properties are given in Tab. 2.3. Using the material properties from Tab. 2.3 we are able to derive the spring constants for the proposed structure and are shown in Tab. 2.4.

k_t	27.02 N mm ⁻¹
k_r	10.7802 N mm ° ⁻¹

Table 2.4: Spring Constants.

The values given in Tab. 2.4 are valid if the structure is homogeneous. This however will not be the case for the final product, since it will be 3D-printed. Due to the print resolution and print-orientation the values could vary throughout the entire structure and possibly exhibit non-linear effects.

Stress and Strain

The structure will be put under stress thus should be able to withstand the forces being measured without rupturing during loading. The stresses and strains were calculated according to Eq. (41)(42)(43)(44) [33].

$$\tau_s = \frac{2T}{\pi ab^2} \quad (41)$$

$$\gamma = \frac{\tau}{G} \quad (42)$$

$$\varepsilon = \frac{\Delta L}{L} \quad (43)$$

$$\sigma = E\varepsilon \quad (44)$$

The resulting stress and strain curves are plotted, with equations (41) and (42) plotted in Fig. 2.14a, and equations (44) and (43) plotted in Fig. 2.14b. The red lines in Fig. 2.14a represent the percentage strain allowed before rupture described as the Elongation at break in Tab. 2.3.

The plots in Fig. 2.14a are given for different whisker length in order to observe in which range the whisker can function at the various length with worry of structural failure. The loading at rupture is given in Tab. 2.5. As for the deflection, it does not cause significant strain on the structure that would lead to rupture. From the plot in Fig. 2.14b it can be seen that the strain values are rather small and nowhere near the elongation at break point.

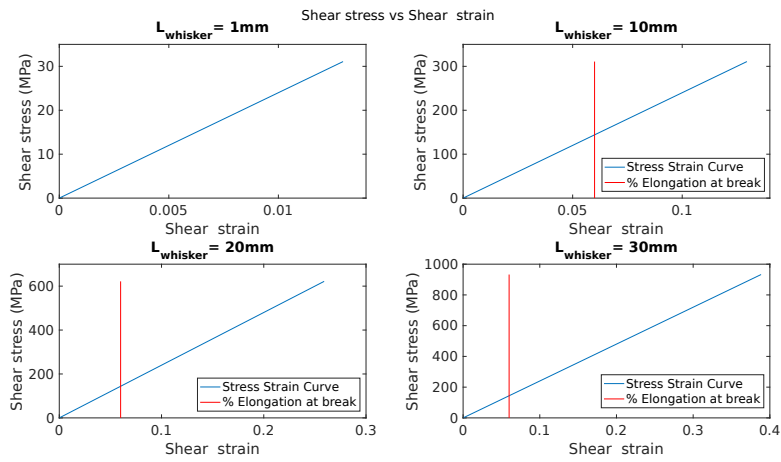


Figure 2.14a: Shear Stress vs Shear Strain (Rotation).

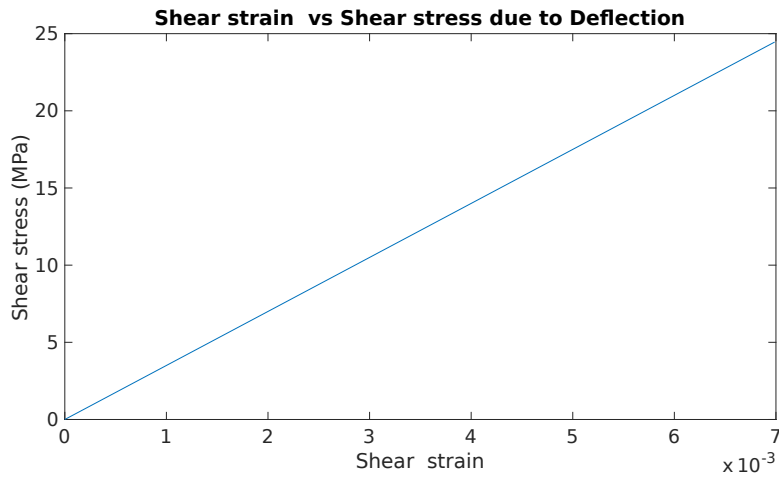


Figure 2.14b: Stress vs Strain (Displacement).

L_{whisker} mm	Load N
1	—
10	23.1
20	11.6
30	7.8

Table 2.5: Force at rupture point during rotation

2.3.2 PCB Patterns

Using the *SCT* method described in Section 2.2.1 the capacitance was further calculated with the dimensions given in Tab. 2.6. It must be noted that these figures were determined prior to the implementation of the *SCT*, they were determined using a simplified *Volume Integration* method elaborated in Ap-

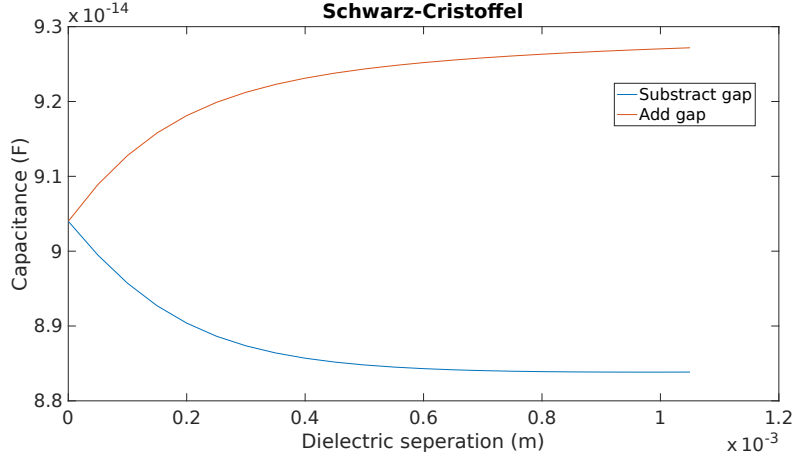


Figure 2.15: Plots for SCT method, 2 ways of calculating total cell Capacitance

Dimension	Value (mm)
w_{trace}	0.2
d	0.4
L	5

Table 2.6: Trace cell Dimensions

pendix A.1. In Fig. 2.15 the capacitance per cell is plotted as a function of the separation gap between the whisker base and the electrodes. The capacitance, in the upper or lower half of the plane, in absence of any dielectric substance is defined as C'_0 . Then the total capacitance for the entire volume in absence of any dielectric will be [20]

$$C_0 = 2C'_0 \quad (45)$$

When a substrate is present, its capacitance is simply added and the total becomes Eq. (46).

$$C_t = 2C'_0 + C_{sub} \quad (46)$$

The capacitance of the additional layers are added to C_t , in accordance to Eq. (37) and (38) [31]. The curve *Add gap* in Fig. 2.15 is plotted using Eq. (47), and the curve *Subtract gap* is plotted using Eq. (48). The equations are similar except for how the capacitance, formed by the air gap as the whisker base moves further away from the electrodes, is added to the total capacitance. Recall that when a dielectric is inserted into an electric field the capacitance of the configuration increases [10], thus we should expect the capacitance in Fig 2.15 to decrease as the separation between the dielectric and the electrodes increases.

$$\frac{1}{C_{ta}} = \frac{1}{L} \left[\frac{1}{C_t + C_{gap}} + \frac{1}{C_{base}} \right] \quad (47)$$

$$\frac{1}{C_{ts}} = \frac{1}{L} \left[\frac{1}{C_t - C_{gap}} + \frac{1}{C_{base}} \right] \quad (48)$$

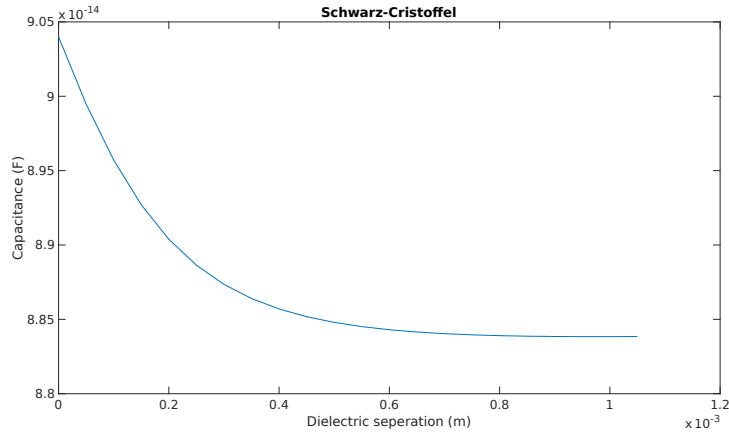


Figure 2.16: Capacitance as function of gap separation (s)

Configuration	Capacitance (F)
C_{air}	3.41×10^{-14}
$C_{dielectric}$	4.64×10^{-14}

Table 2.7: Capacitance asymptotes

Eq. (47) is derived from the steps presented in [31], however the configurations presented in their paper are used for multi-layered dielectrics. And the situation is not presented where an intermediate layer is composed of air. In our case we make the assumption that the capacitance due to air is already counted in C_t . Thus as the gap between the electrodes and whisker base increases, using Eq. (47), its corresponding capacitance would be counted double. Thus our solution is to subtract that capacitance from the total, leading to Eq. (48) and the *Subtract gap* plot in Fig. 2.15. Eq. (48) is plotted again for convenience in Fig. 2.16. The asymptotes for the capacitance values are given in Tab. 2.7. The maximum asymptote is approximately half of the maximum shown in Fig. 2.8, but this is due to the aforementioned relative difference between the capacitance of the two methods shown in Fig. 2.11. The minimum asymptote is also less than half the minimum shown in Fig. 2.8, though it is uncertain to what value the plot tends.

Electrode Patterns

The two chosen designs for the PCB trace are shown in Fig. 2.17a and 2.17b, and the final board layout in Appendix C, which are inter-digital and spiral electrode patterns respectively. The inner-square represents the area under the structure shown in Fig. 2.12. From the capacitance calculation in the previous section we

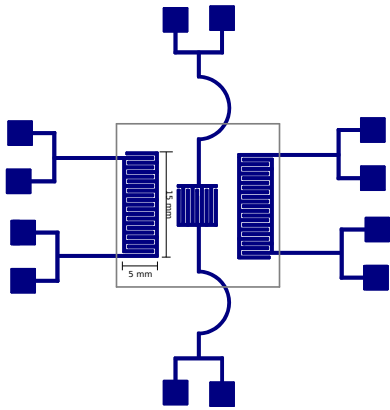


Figure 2.17a: Inter-digital traces

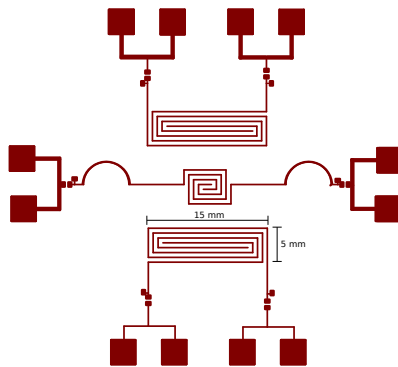


Figure 2.17b: Spiral trace pattern

could see that the capacitance is proportional to the length of the trace. For this reason the spiral and inter-digital traces were chosen as these could be used to maximize the length within a small area. A small trace width and gap between traces is preferred as this would take up less space, thus more capacitors can be added within a smaller area effectively increasing the sensitivity as well. Using the capacitance calculated and taking into account the difference in lengths, the spiral electrodes should have a capacitance increase of a factor of 35 and for the inter-digital electrodes a factor of 20 for the larger pads.

2.3.3 Discussion

The proposed structure outlined in this section can be described by the model analyzed in Section 2.1. The beams which support the whisker base allow for the 2 degrees of freedom needed to determine the contact location of the force along the whisker. Another element which was considered in the design was the area which is to be used as dielectric for the capacitance measurement. The area was maximized to fit within the structure's base without inhibiting lateral movement of the base. For this design PLA will be used due to its availability and elastic properties. Due to the proposed function of the model the stress and strain characteristics were also investigated and a range of possible maximum loads at a given contact location were listed in Tab. 2.5 Capacitive sensing is used for this design. From the calculation it was shown that the capacitance is linearly proportional to the length. With this in mind we optimized the capacitor dimensions to increase its length within a given boundary. This led to the electrode patterns shown in Fig. 2.17a, and 2.17b.

2.3.4 Conclusion

The designed structure will have 2 degrees of freedom of which the range of movement will be determined by the cross-section and length of the support beams. The rotation angle of the base will lead to observable change in the capacitance if the gap between the dielectric and the electrodes is kept less than 1 mm high. The support beams will be able to withstand loading up to 23 N at a contact length of 10 mm. With increasing contact length the loading should be kept minimal to avoid rupturing the support beams.

3 Fabrication

3.1 Structure

The structure was designed using the Openscad cad-drawing software. The advantage of the program is that it is possible to design fully parameterized structures which can be easily scaled and adapted to the users wishes. The design code for the model is given in Appendix F.

3.1.1 Objet

The first iteration was printed with the *Objet Eden 250* printer. It is a Polyjet printer which, much like ink-jet printers, jet layers of photo-polymer onto a print-bed. The jetted polymer is then uv-cured in order to harden, so that the next layer can be deposited on top. By this process it is able to achieve a layer resolution of 16 μm . Due to the design of the structure, printing a robust whisker on the base would require support material during the printing process which would later be removed in post-processing. The whisker extension ruptured at the base for this iteration, for this reason subsequent prints were made without the whisker for testing. This would also save on material and print time. Print times were quite long using the Objet, they were in the range of several hours not including post-processing for removing the support material. The support material is different from the actual print material, and is removed chemically after printing. Furthermore the material used in the Objet, *VeroClear* is costly as well, which is around €190 per kg. The final product weighed approximately 20g, which would work out to €3.80 not including the support material as this was not weighed.

3.1.2 Ultimaker

The subsequent prints were done using the *Ultimaker 2* which has a resolution of 100 μm . The material used was PLA which averages around €30 per kg, thus around €0.60. Prints using the Ultimaker were printed in much less time, approximately $\frac{1}{3}$ of the time used by the Objet. However this is at cost of resolution, and the support material would be the same as the actual print material. This would have to be printed in a way which would allow it to be removed easily afterwards, as the support and print material is the same. Removing the support material chemically would be a challenge as you would have to find a way to control the way each part is being removed.

3.1.3 Print Orientation

Different layer thicknesses and print orientation have an effect on the mechanical properties of 3D-printed structures. The print orientation has the largest effect on the strains which act on the structure. Thus the print orientation would determine the robustness of the structure [35]. When printing the model, special attention must be made to how the whisker is printed. In the design, the whisker is elongated vertically. If the whisker is printed with layers stacked vertically it will be much more susceptible to rupturing when bent along the vertical axis. Thus when printing the final structure, ideally the structure should be printed at an angle which optimizes the robustness of the whisker

PCB

The electrode pattern was designed in Eagle Cad software, with the final model shown in Appendix C. The PCB was then ordered from a 3rd party. This fabrication process steps are found with the respective company [36].

3.2 Discussion

For the fabrication of this prototype focus was placed on a test prototype for the measurements. In the first iterations the whisker ruptured at the base of the model. Therefore to avoid the issue with print-orientation and rupturing of the whisker, the whisker support structure was printed independently. In order to minimize prototyping cost and print time, it was opted to make use of the Ultimaker 2 printer with PLA material. The PCB electrodes were placed on a two sided board in order to be able to test the two electrode configuration.

3.3 Conclusion

Using the Ultimaker printer we are able to develop multiple prototypes with reduced time and costs. Moreover the fabrication method in this case is focused primarily on testing the viability of the functioning of the proposed whisker sensor. Therefore the results of the model may vary to some degree when the whisker is printed directly to the structure.

4 Measurement and Results

4.1 Validation Method

Mechanical test

The mechanical characteristics were measured using a Sylvac D80 displacement measurement probe which is accurate within $0.1\ \mu\text{m}$. The Probe has a spring constant of $0.03\ \text{N mm}^{-1}$ which is removed from the final result. With a pulley set-up and several weights the mechanical characteristics are able to be determined. A diagram of the measurement setup for the rotation measurement is shown in Fig. 4.1a and 4.1b. Connecting the unit to a PC with a serial connection we were able to measure real-time data.

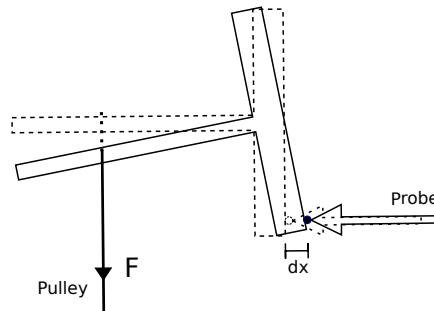


Figure 4.1a: Setup for measuring rotation angle.

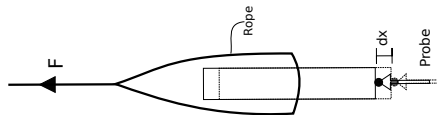


Figure 4.1b: Setup for measuring displacement.

Capacitance

To determine the capacitance an LCR-meter is used. Due to the low ranges expected for measurement an *HP4284A* meter will be used which has a resolution down to $0.01\ \text{fF}$. The capacitance will be measured with the whisker base completely absent. After which subsequent measurements will include the whisker base, measuring the capacitance with the base at different distances from the electrodes. This will help determine the optimal height at which to place the whisker base. Should the results be promising then measurements will be done to relate the rotation of the whisker base to the change in capacitance.

4.2 Mechanical Dynamics

4.2.1 Rotation and Translation

In Fig. 4.2b and 4.2a, the measured *vs.* expected rotation and displacements are plotted as function of the force. And further in Fig. 4.2c and 4.2d the spring constants are plotted relative to the expected spring constants.

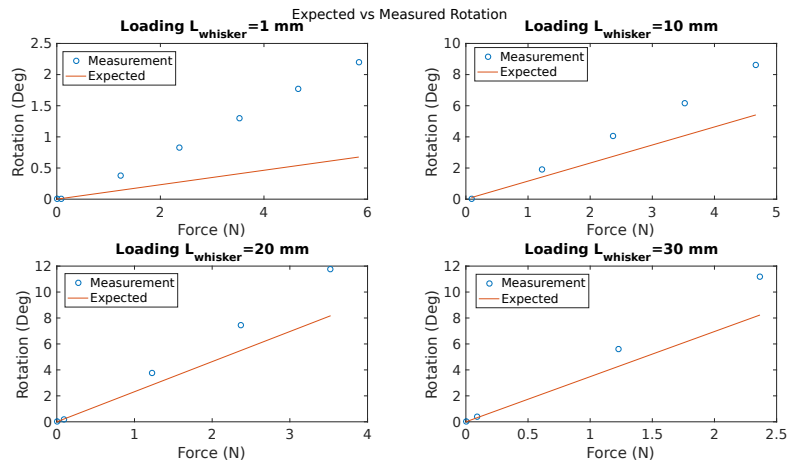


Figure 4.2a: Measured vs Expected Twist Angle.

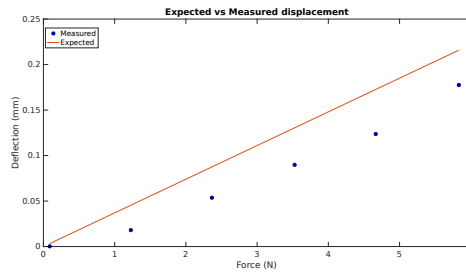


Figure 4.2b: Measured vs Expected Displacement.

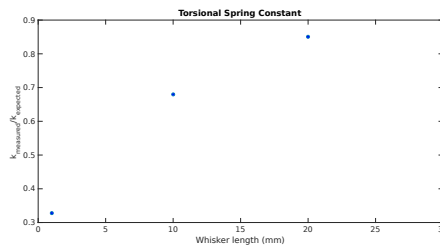


Figure 4.2c: Torsional Spring constant vs Length.

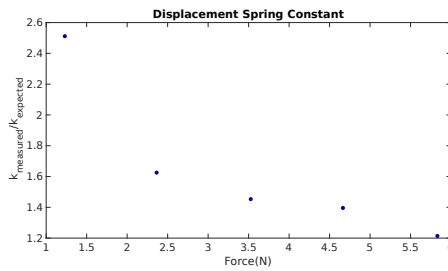


Figure 4.2d: Spring constant vs Force.

Discussion

In Fig. 4.2a the twist angle *vs.* force is plotted for various whisker lengths. From the plots we see that the measurement differs from the expected results, moreover as the length increase the difference reduces. As for the displacement, the measurement differs slightly from the expected results. When investigating the relative difference between the expected and measured spring constants we see, for both the rotation and displacement, non-linearity. In the case of the rotation it is non-linear relative to the whisker length, thus the force contact location. As for the displacement it shows non-linearity w.r.t. the force. These non-linear effects could be due to the print-orientation and bonding between print layers.

4.2.2 Hysteresis

Throughout the measurements hysteresis was observed and is plotted for one measurement in Fig. 4.3b and 4.3a.

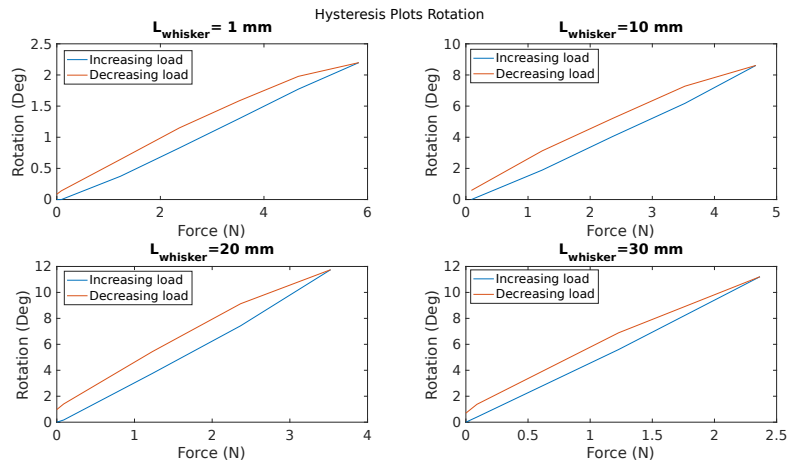


Figure 4.3a: Rotation Hysteresis

Discussion

The structure showed a significant amount of hysteresis as shown in the figure.

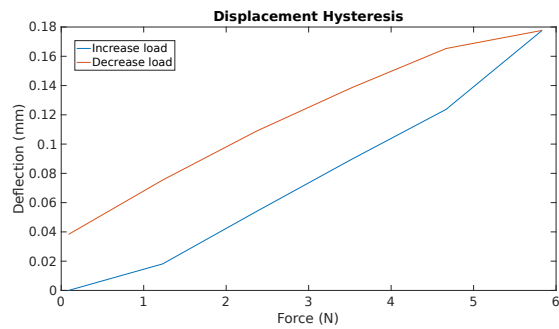


Figure 4.3b: Displacement Hysteresis

Furthermore structure was rarely observed to return to its initial position. Prior to each measurement the structure had to be manually reset.

4.2.3 Creep

Creep is an inherent property of viscoelastic polymers, and it was possible to observe this in the measurements. The creep measurement was done over a period of 2 mins. Fig. 4.4b shows the displacement creep at the base of the structure and Fig. 4.4a shows the creep for whisker length of 30 mm.

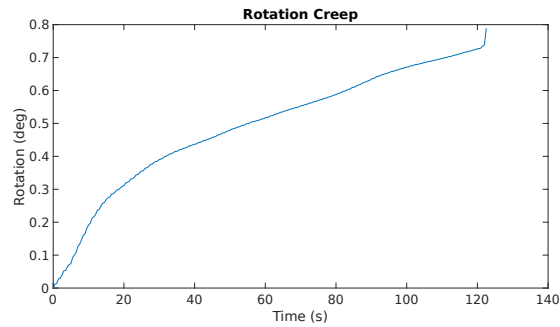


Figure 4.4a: Rotation Creep

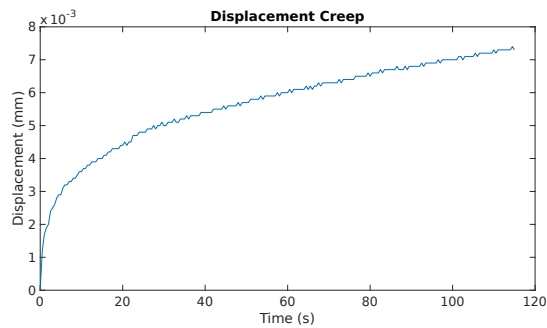


Figure 4.4b: Displacement Creep

Discussion

From Fig. 4.4b we notice that even-though the displacement is quite small, in the micrometers, the creep is still quite noticeable over the given time range and is still rising after the pre-set time. The creep in Fig. 4.4a is very noticeable in the measurements, the structure twists an additional 1° over the pre-set time.

4.3 Capacitance

Due to time constraints no measurements were done on the electrode patterns. This will be left as a future task for the prototype

4.4 Complete Prototype

NOT COMPLETED

4.5 Conclusion

From the measurements we have shown that the structure is viable, with 2 degrees of freedom i.e. lateral and rotational movement. The lateral displacement ranges in the micrometers due to the design, the rotation however was measured to reach up to 12° with a particular whisker length and load below the rupture load. The model does exhibit non-linear effects for both degrees of freedom, which could be both due to the print-orientation and the material properties.

5 Discussion

The design proposed in this paper is intended to function as a whisker which mimics that of a rat. The forces and moments at the whisker base were modeled to be measured using the capacitance of a PCB. Focus was placed on testing the viability of the base structure, therefore the mechanical characteristics for varying print-orientation and print-layer resolution were not thoroughly investigated. The model is designed with little freedom of motion for lateral displacement, and optimized for rotation. This was done by configuring the spring constants in the respective degrees of freedom. Testing the mechanical structure revealed some interesting results. Primarily the severity of the non-linearity of the spring constants *w.r.t.* the force and whisker length. This is believed to be due to the fact that the structure is not homogeneous i.e., it is printed in layers. Moreover the material itself is a viscoelastic polymer which does exhibit observable effects of creep and hysteresis as was described in the measurement results in Section 4. This non-linearity however could be exploited in the capacitive measurement, as different contact forces, or contact lengths would produce a non-linear change of the air gap separation distance. Moreover a model for the capacitance is proposed which is optimized for measuring the rotational movement. The change in capacitance for lateral displacement was not thoroughly investigated, thus no model has yet been proposed.

6 Conclusion

In this paper the viability of designing a whisker transducer with 2-DOF was investigated. Measuring the movements using the capacitance induced by the electrode traces of a PCB. The basic structure was 3D-printed using PLA material, on the Ultimaker 2. For the prototype, only the base structure was printed and tested thus in absence of the whisker. With this setup the effects of print-orientation on the mechanical properties were not thoroughly investigated. It is expected however that the print orientation will have an effect on the maximum loading and the mechanical response of the structure. The prototype only has one noticeable degree of freedom, this is due to the inherent design of the structure of the model. The creep and hysteresis exhibit noticeable effects in the measurements. The structure rarely returned to its initial position, which would show that energy is being stored in the system. The hysteresis and creep effects could influence the value of the measured capacitance if they are not taken into account. Moreover the structure showed significant non-linearity during operation *w.r.t.* the spring constants of the system. As mentioned previously these non-linearity could be due both to the print-orientation, material, and also the print resolution. The method for calculating the capacitance should still be refined as there are still some uncertainties in the model which have been mentioned in previously in Section 2.3.2. The use of the asymptote method provides an expected range for the capacitance, which coincides reasonably well with some values given by the SCT-method. Based on the aforementioned points, the prototype is viable however the discussed improvements should be considered and implemented.

6.1 Recommendation

The prototype in this paper is poorly optimized for a second degree of freedom. The model allows for ample rotation, however lateral movement is restricted. In order to increase the movement, one of the whisker supports could be removed, theoretically this should allow a displacement increase of a factor of at least 4, not taking into account non-linear effects. It would be interesting to investigate what effects changing the print-orientation will have on the mechanical characteristics of the structure. Measurements should be done on the current electrode pattern to determine the accuracy of the model described in Section 2.2.1. Moreover the capacitive measurement of the motion in the second domain of freedom should be investigated. With the proposed SCT analysis method it should be possible to derive an equivalent model of the system. From the simulated models it was shown that the capacitance values are small. A focus should be placed in increasing both the overall capacitance, and its sensitivity to the change in air-gap. The sensitivity however can be increased by using a larger rotation arm, as well as using a material with a larger dielectric constant. Another area of research can be investigating how to print the material in order to withstand larger loads. This is especially valid for the whisker structure itself, as with the prototypes printed the whisker was easily ruptured. A possible solution would be to print the parts individually and later connect them. This would allow both the base and the whisker to be printed in orientations which would offer more support and allow them to withstand larger loading.

References

- [1] G. Dehnhardt, B. Mauck, and H. Bleckmann, “Seal whiskers detect water movements,” *Nature*, vol. 394, no. 6690, pp. 235–236, 1998.
- [2] J. A. Birdwell, J. H. Solomon, M. Thajchayapong, M. A. Taylor, M. Cheely, R. B. Towal, J. Conradt, and M. J. Hartmann, “Biomechanical models for radial distance determination by the rat vibrissal system,” *Journal of Neurophysiology*, vol. 98, no. 4, pp. 2439–2455, 2007.
- [3] T. J. Prescott, M. J. Pearson, B. Mitchinson, J. C. W. Sullivan, and A. G. Pipe, “Whisking with robots from rat vibrissae to biomimetic technology for active touch,” *IEEE Robotics and Automation Magazine*, vol. 16, no. 3, pp. 42–50, 2009.
- [4] B. W. Quist, V. Seghete, L. A. Huet, T. D. Murphey, and M. J. Hartmann, “Modeling forces and moments at the base of a rat vibrissa during noncontact whisking and whisking against an object,” *The Journal of Neuroscience*, vol. 34, no. 30, pp. 9828–9844, 2014.
- [5] R. B. Towal and M. J. Hartmann, “Principles and applications of active tactile sensing strategies in the rat vibrissal system,” in *Sensors, 2010 IEEE*, pp. 2230–2234, IEEE, 2010.
- [6] S. Ready, G. Whiting, and T. N. Ng, “Multi-material 3d printing,” in *NIP & Digital Fabrication Conference*, vol. 2014, pp. 120–123, Society for Imaging Science and Technology, 2014.
- [7] F. Ju and S.-F. Ling, “A micro whisker transducer with sensorless mechanical impedance detection capability for fluid and tactile sensing in space-limited applications,” *Sensors and Actuators A: Physical*, vol. 234, pp. 104–112, 2015.
- [8] O. Bebek and M. C. Cavusoglu, “Whisker sensor design for three dimensional position measurement in robotic assisted beating heart surgery,” in *Robotics and Automation, 2007 IEEE International Conference on*, pp. 225–231, IEEE, 2007.
- [9] M. H. Evans, C. W. Fox, N. F. Lepora, M. J. Pearson, J. C. Sullivan, and T. J. Prescott, “The effect of whisker movement on radial distance estimation: a case study in comparative robotics,” *Active Touch Sensing*, p. 106, 2014.
- [10] R. P. Feynman, R. B. Leighton, and M. Sands, *The Feynman Lectures on Physics, Desktop Edition Volume II*, vol. 1. Basic books, 2013.
- [11] N. Izadi, “Bio-inspired mems aquatic flow sensor arrays,” 2011.
- [12] C. Barbier, J. A. Humphrey, J. Paulus, and M. Appleby, “Design, fabrication and testing of a bioinspired hybrid hair-like fluid motion sensor array,” in *ASME 2007 International Mechanical Engineering Congress and Exposition*, pp. 1319–1324, American Society of Mechanical Engineers, 2007.

- [13] J. Stocking, W. Eberhardt, Y. Shakhsher, B. Calhoun, J. Paulus, and M. Appleby, "A capacitance-based whisker-like artificial sensor for fluid motion sensing," in *Sensors, 2010 IEEE*, pp. 2224–2229, IEEE, 2010.
- [14] N. Izadi, R. Jaganatharaja, J. Floris, and G. Krijnen, "Optimization of cricket-inspired, biomimetic artificial hair sensors for flow sensing," *arXiv preprint arXiv:0802.3768*, 2008.
- [15] M. J. Hartmann, N. J. Johnson, R. B. Towal, and C. Assad, "Mechanical characteristics of rat vibrissae: resonant frequencies and damping in isolated whiskers and in the awake behaving animal," *The Journal of neuroscience*, vol. 23, no. 16, pp. 6510–6519, 2003.
- [16] D. J. Griffiths and R. College, *Introduction to electrodynamics*, vol. 3. prentice Hall Upper Saddle River, NJ, 1999.
- [17] N. I. Dib, *Theoretical characterization of coplanar waveguide transmission lines and discontinuities*. PhD thesis, 1992.
- [18] W. J. Gibbs, *Conformal transformations in electrical engineering*. Chapman & Hall, 1958.
- [19] Wikipedia, "Cauchy–riemann equations:conformal mapping." https://en.wikipedia.org/wiki/Cauchy%E2%80%93Riemann_equations#Conformal_mappings, 2016. Accessed: 27-Apr-2016.
- [20] "Chapter-3 : Conformal mapping - an overview." http://shodhganga.inflibnet.ac.in/bitstream/10603/28373/10/10_chapter%203.pdf. Accessed: 27 Apr 2016.
- [21] W. Hilberg, "From approximations to exact relations for characteristic impedances," *Microwave Theory and Techniques, IEEE Transactions on*, vol. 17, no. 5, pp. 259–265, 1969.
- [22] R. Igreja and C. Dias, "Analytical evaluation of the interdigital electrodes capacitance for a multi-layered structure," *Sensors and Actuators A: Physical*, vol. 112, no. 2, pp. 291–301, 2004.
- [23] H. Da-Wei, C. Xin-Hong, W. Zhong-Jian, X. Da-Wei, S. Zhao-Rui, and Y. Yue-Hui, "An analytical model for coplanar waveguide on silicon-on-insulator substrate with conformal mapping technique," *Chinese Physics B*, vol. 20, no. 1, p. 010210, 2011.
- [24] C. R. E., *Field theory of guided waves*. New York: McGraw-Hill Book Company Inc, 1960.
- [25] W. Mathworld, "Elliptic modulus." <http://mathworld.wolfram.com/EllipticModulus.html>, 2016. Online; accessed 27-Apr-2016.
- [26] T. Sun, N. G. Green, S. Gawad, and H. Morgan, "Analytical electric field and sensitivity analysis for two microfluidic impedance cytometer designs," *Iet Nanobiotechnology*, vol. 1, no. 5, pp. 69–79, 2007.

- [27] T.-T. Ngo, A. Bourjilat, J. Claudel, D. Kourtiche, and M. Nadi, “Design and realization of a planar interdigital microsensor for biological medium characterization,” in *Next Generation Sensors and Systems*, pp. 23–54, Springer, 2016.
- [28] T. Sun, N. G. Green, and H. Morgan, “Electric field analysis using schwarz-christoffel mapping,” in *Journal of Physics: Conference Series*, vol. 142, p. 012029, IOP Publishing, 2008.
- [29] M. Vukadinovic, B. Malic, M. Kosec, and D. Krizaj, “Modelling and characterization of thin film planar capacitors: inherent errors and limits of applicability of partial capacitance methods,” *Measurement Science and Technology*, vol. 20, no. 11, p. 115106, 2009.
- [30] E. Carlsson and S. Gevorgian, “Conformal mapping of the field and charge distributions in multilayered substrate cpws,” *Microwave Theory and Techniques, IEEE Transactions on*, vol. 47, no. 8, pp. 1544–1552, 1999.
- [31] S. O. Blume, R. Ben-Mrad, and P. E. Sullivan, “Modelling the capacitance of multi-layer conductor-facing interdigitated electrode structures,” *Sensors and Actuators B: Chemical*, vol. 213, pp. 423–433, 2015.
- [32] H. Droogendijk, J. Casas, T. Steinmann, and G. Krijnen, “Performance assessment of bio-inspired systems: flow sensing mems hairs,” *Bioinspiration & biomimetics*, vol. 10, no. 1, p. 016001, 2014.
- [33] W. C. Young and R. G. Budynas, *Roark’s formulas for stress and strain*, vol. 7. McGraw-Hill New York, 2002.
- [34] MakeItFrom, “Polylactic (pla, polylactide).” <http://www.makeitfrom.com/material-properties/Polylactic-Acid-PLA-Polylactide/>, Apr 2016.
- [35] A. Farzadi, M. Solati-Hashjin, M. Asadi-Eydivand, and N. A. A. Osman, “Effect of layer thickness and printing orientation on mechanical properties and dimensional accuracy of 3d printed porous samples for bone tissue engineering,” *PloS one*, vol. 9, no. 9, p. e108252, 2014.
- [36] WEDirekt, “Pcb.” <http://www.wedirekt.nl/nl/pcb>, Apr 2016.

A Capacitance Calculations

A.1 Volume integral

This method could give an estimate of the order of magnitude of the actual capacitance. In the dielectric region the relative \vec{D} field is determined by the polarization in the material which is parallel to the direction of the electric field. In this method the integration interval for the energy is split into several intervals as shown in Fig. A.1 Keeping in mind the requirement for an equipotential on the surface of the conductor, the charge Q is derived using the average electric field magnitude along the surface (49).

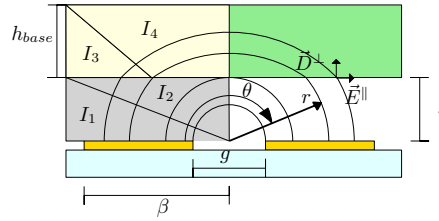


Figure A.1: Integration Intervals

$$E_{\text{avg}} = \frac{2\Delta\Phi}{\pi\beta} \quad (49)$$

The same is done for the dielectric region keeping in mind the different values of r in this region along with the dielectric constant ϵ_r . Keeping in mind Eq. (16) and (17), we can derive a relation for the angle at the interface, the derivation of the relation is given below.

$$E_{\text{air}}^{\parallel} = |E| \sin(\theta_{\text{air}})$$

$$D_{\text{air}}^{\perp} = \epsilon_0 |E| \cos(\theta_{\text{air}})$$

$$E_{\text{d}}^{\parallel} = |E| \sin(\theta_{\text{d}})$$

$$D_{\text{d}}^{\perp} = \epsilon_{\text{d}} |E| \cos(\theta_{\text{d}})$$

$$E_{\text{air}}^{\parallel} = E_{\text{d}}^{\parallel}$$

$$D_{\text{air}}^{\perp} = D_{\text{d}}^{\perp}$$

$$\frac{E_{\text{air}}^{\parallel}}{D_{\text{air}}^{\perp}} = \frac{E_{\text{d}}^{\parallel}}{D_{\text{d}}^{\perp}}$$

$$\frac{1}{\epsilon_0} \tan(\theta_{\text{air}}) = \frac{1}{\epsilon_0 \epsilon_r} \tan(\theta_{\text{d}})$$

Using cylindrical coordinates the volume integral is set up for the interval I_1 . Refer to Fig. A.1 for parameter description.

$$\frac{g}{2} < r < \frac{\beta}{\cos(\theta)} \quad (50)$$

$$0 < \theta < \tan^{-1}\left(\frac{s}{\beta}\right) \quad (51)$$

$$0 < z < L \quad (52)$$

The integral then follow (53), which is then split into the \vec{E} term and \vec{D} term such that the sum of the two integral equal U_1 . The rest calculations which follow are related to the displacement field term of the first interval.

$$U_1 = \frac{\epsilon_0}{2} \int_z \int_\theta \int_r (\epsilon_r E_{\text{air}}^2{}^\perp + E_{\text{air}}^2{}^\parallel) r d\theta dr dz \quad (53)$$

Let Y_1 denote the integral of the displacement field $D_{\text{air}}{}^\perp$ and recall Eq. (15).

$$Y_1 = \frac{\epsilon_0}{2} \int_\theta \int_r \int_z |E|^2 \cos^2(\theta) r dz dr d\theta \quad (54)$$

$$= \frac{L\epsilon_0}{2} \left| \frac{\Delta\Phi}{\pi} \right|^2 \int_\theta \int_r \frac{\cos^2(\theta)}{r} dr d\theta \quad (55)$$

$$= \frac{L\epsilon_0}{2} \left| \frac{\Delta\Phi}{\pi} \right|^2 \int_\theta \cos^2(\theta) \ln \frac{2\beta}{g \cos(\theta)} d\theta \quad (56)$$

There are no analytical solutions using standard functions to Eq. 56. Using numerical solvers such as Mathematica gives a result which is complex and with Polylogarithmic functions. Parameterizing θ as a function of r yields a similar integral.

B Model

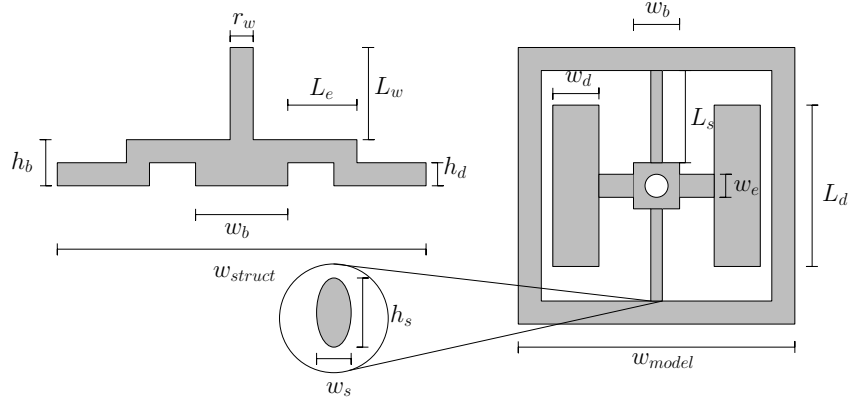


Figure B.1: Whisker model dimensions

Parameter	Dimension mm
r_w	2
L_w	50
L_e	5
w_e	2.5
h_b	4
w_b	5
w_{model}	30
w_{struct}	20
h_d	2
L_d	15
w_d	5
h_s	3.2
w_s	1.6
L_s	8

Table B.1: Whisker structure dimension.

C PCB Layout

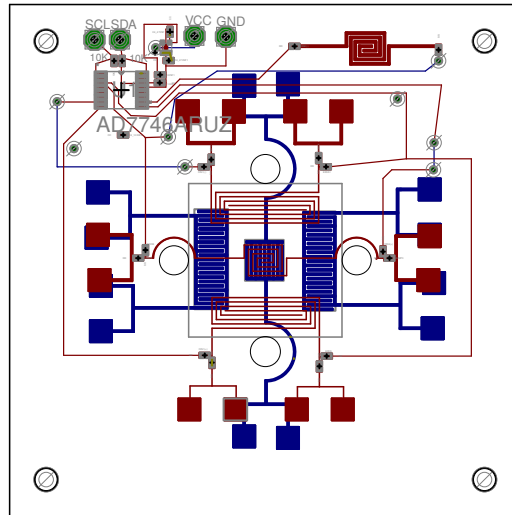


Figure C.1: Board layout.

D 3D Prints

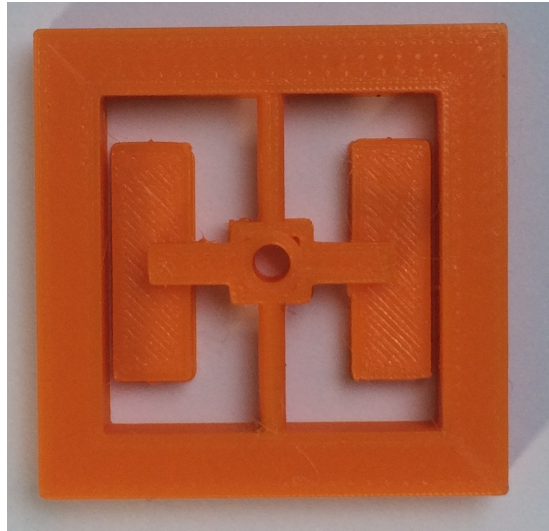


Figure D.1a: PLA printed test structure.

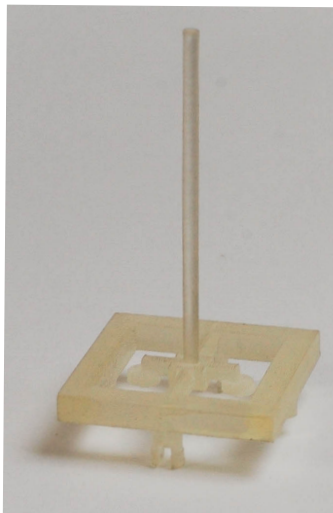


Figure D.1b: Veroclear printed test structure.

E Matlab Code

```

%%
%%%%%%%%%%%%%%%%%%%%%%%%%%%%%%%%%%%%%%%%%%%%%%%%%%%%%%%%%%%%%%%%%%%%%%%%
%%%%%%%%%%%%%%%%%%%%%%%%%%%%%%%%%%%%%%%%%%%%%%%%%%%%%%%%%%%%%%%%%%%%%%%% ...
Capacitor %%%%%%%%%%%%%%%%%%%%%%%%%%%%%%%%%%%%%%%%%%%%%%%%%%%%%%%%%%%%%%%%%%%%%%%%%
%%%%%%%%%%%%%%%%%%%%%%%%%%%%%%%%%%%%%%%%%%%%%%%%%%%%%%%%%%%%%%%%%%%%%%%%
clc
clear all;
close all;
format shorte
%%
e0 = 8.85418782e-12;           % relative permittivity vacuum
er = 2.5;                     % relative permittivity whisker base
esub = 5;                     % relative permittivity of substrate
s = 0:0.05e-3:1.05e-3;       % gap between electrodes and ...
    whisker base
% dv = 0.05e-3:0.05e-3:5e-3;   % distance between electrodes
% twv = 0.05e-3:0.05e-3:5e-3;  % width of electrode traces
d = 0.4e-3;
tw = 0.2e-3;
tsub = 1.55e-3;               % PCB substrate thickness
L = 5e-3;                     % length of electrode
bh = 2e-3;                    % thickness of whisker base
% [d,tw] = meshgrid(dv,twv);
beta = d./2 + tw;
V = 0.5;                       % potential difference ...
    between electrode
n =50;                         % number of contour lines
%%
%%% Asymptote method%%
Cair = e0*L.*log(2.*beta./d)/(2*pi);           % Capacitance in ...
    free space (no dielectric) (single side)
Cdie = e0*er*L.*log(2.*beta./d)/(2*pi);       % Capacitance due ...
    to dielectric (no air gap)
Csub = e0*esub*L.*log(2.*beta./d)/(2*pi);
Ca0 = 2*Cair + Csub;
Ctotd= 2*Cair + Cdie + Csub;                   % total ...
    capacitance with dielectric
Ctot0=2*Cair + Csub;                           %total ...
    cap no dielectric
%%
%%% Schwarz-Cristoffel
a = tw./2;                                     % half elctrode width
h1 = s;                                        % height first layer (air gap)
h2 = s + bh;                                  % height second layer ...
    (whisker base)
h3 = tsub;                                     % height substrate layer

% Elliptical moduli
%no back conducting plate
k0 = a./(a + d);
k1 = ( sinh( (pi.*a)/(2.*h1) ) ) ./ ( sinh( ...
    (pi*(a+d))/(2.*h1) ) );
k2 = ( sinh( (pi.*a)/(2.*h2) ) ) ./ ( sinh( ...
    (pi*(a+d))/(2.*h2) ) );
k3 = ( sinh( (pi.*a)/(2.*h3) ) ) ./ ( sinh( ...
    (pi*(a+d))/(2.*h3) ) );

% with back conducting plate

```

```

% k0 = a./(a + d);
% k1 = ( tanh( (pi.*a)./(2.*h1) ) ) ./ ( tanh( ...
    (pi*(a+d))./(2.*h1) ) );
% k2 = ( tanh( (pi.*a)./(2.*h2) ) ) ./ ( tanh( ...
    (pi*(a+d))./(2.*h2) ) );
% k3 = ( tanh( (pi.*a)./(2.*h3) ) ) ./ ( tanh( ...
    (pi*(a+d))./(2.*h3) ) );

% complimentary moduli
k0p = sqrt(1 - k0.^2) ;
k1p = sqrt(1 - k1.^2) ;
k2p = sqrt(1 - k2.^2) ;
k3p = sqrt(1 - k3.^2) ;

% preallocate space
KK0 = ones(size(k0));
KK1 = ones(size(k1));
KK2 = ones(size(k2));
KK3 = ones(size(k3));

%% Determine K(k)/K(k')
for i=1:size(k0,1)
    for j=1:size(k0,2)
        if k0(i,j) > 0
            if k0(i,j) <= 1/sqrt(2)
                KK0(i,j) = pi ./ ( log( 2.*( ...
                    (1+sqrt(k0p(i,j)))./(1-sqrt(k0p(i,j)))) ) ) ...
                );
            elseif k1(i,j) <= 1
                KK0(i,j) = ( log( 2.*( ...
                    (1+sqrt(k0(i,j)))./(1-sqrt(k0(i,j)))) ) ) ) ./ pi;
            end
        else
            KK0(i,j) = 0;
        end
    end
end
for i=1:size(k1,1)
    for j=1:size(k1,2)
        if k1(i,j) > 0
            if k1(i,j) <= 1/sqrt(2)
                KK1(i,j) = pi ./ ( log( 2.*( ...
                    (1+sqrt(k1p(i,j)))./(1-sqrt(k1p(i,j)))) ) ) );
            elseif k1(i,j) <= 1
                KK1(i,j) = ( log( 2.*( ...
                    (1+sqrt(k1(i,j)))./(1-sqrt(k1(i,j)))) ) ) ) ./ pi;
            end
        else
            KK1(i,j) = 0;
        end
    end
end
for i=1:size(k2,1)
    for j=1:size(k2,2)
        if k2(i,j) > 0
            if k2(i,j) <= 1/sqrt(2)
                KK2(i,j) = pi ./ ( log( 2.*( ...
                    (1+sqrt(k2p(i,j)))./(1-sqrt(k2p(i,j)))) ) ) );
            elseif k2(i,j) <= 1
                KK2(i,j) = ( log( 2.*( ...
                    (1+sqrt(k2(i,j)))./(1-sqrt(k2(i,j)))) ) ) ) ./ pi;
            end
        end
    end
end

```

```

        else
            KK2(i,j) = 0;
        end
    end
end
for i=1:size(k3,1)
    for j=1:size(k3,2)
        if k3(i,j) > 0
            if k3(i,j) <= 1/sqrt(2)
                KK3(i,j) = pi./ ( log( 2.*( ...
                    (1+sqrt(k3p(i,j)))./((1-sqrt(k3p(i,j)))) ) ) ) ;
            elseif k3(i,j) <= 1
                KK3(i,j) = ( log( 2.*( ...
                    (1+sqrt(k3(i,j)))./((1-sqrt(k3(i,j)))) ) ) )./pi;
            end
        else
            KK3(i,j) = 0;
        end
    end
end
end
%%
C0 = 4*e0.*KK0;
Cg = 2*e0.*KK1;%2*e0*(er-1).*KK1;
Cd = 2*e0*er.*KK2;
Csub = 2*e0*esub.*KK3;

Ctots = 1./(1./(2*C0 + Csub - Cg) + 1./Cd)*L;
Ctots2 = 1./(1./(2*C0 + Csub + Cg) + 1./Cd)*L;

% Err = Ctots./Ctota;
%% plots
close all
figure
% contour3(d,tw,Ctots,n);
% view(-26,24);
% xlabel({'Seperation between taces (m)'});
% ylabel({'Trace width(m)'});
% zlabel({'Capacitance (F)'});
plot(s,Ctots,s,Ctots2);
% line([0 2e-3],[Ctotal Ctota1],'color','red');
% line([0 2e-3],[Ctota2 Ctota2])
legend('Substract gap','Add gap')
xlabel('Dielectric seperation (m)');
ylabel('Capacitance (F)');
title('Schwarz-Cristoffel');

%%
figure
contour3(d,tw,Ctotal,n);
view(-26,24);
xlabel({'Seperation between taces (m)'});
ylabel({'Trace width (m)'});
zlabel({'Capacitance (F)'});
% plot(s,Ctota);
% xlabel('Distance from dielectric (m)');
% ylabel('Capacitance (F)');
title('Asymptote method');

%%
E = Ctota0./Ctots;
% D = Ctots./Ctotd;
figure

```

```

contour3(d,tw,E,n);
xlabel({'Seperation between taces (m)'});
ylabel({'Trace width(m)'});
zlabel({'Relative difference Cas/CSCT'}) ;

clc;
clear all;
close all;
%%
%%%%%%%%%%%%%%%%%%%%%%%%%%%%%%%%%%%%%%%%%%%%%%%%%%%%%%%%%%%%%%%%%%%%%%%%
Mechanics %%%%%%%%%%%%%%%%%%%%%%%%%%%%%%%%%%%%%%%%%%%%%%%%%%%%%%%%%%%%%%%%%%%%%%%%%
%%%%%%%%%%%%%%%%%%%%%%%%%%%%%%%%%%%%%%%%%%%%%%%%%%%%%%%%%%%%%%%%%%%%%%%%
%% Elliptical cross section
flex_strength = 80;          % max flexural stress for material MPa
t_max = 60;                 % Max tensile stress MPa
elong_break = 0.06;        % elongation at break points
E = 3.5e3;                  % Young's Modulus MPa
G = 2.4e3;                  % Shear Modulus MPa
lw = [1; 10 ;20 ;30];      % Whisker length
ls = 8;                     % Distance from ...
    support base to outer square
mi = 1.6;                   % minor axis
ma = 3.2;                   % major axis
Fs = 0.1:0.1:25;           % Force
Mx = lw*Fs;                 % Generated Torque
Ksenr = 0.03/atan(1/ls);    % Measuring ...
    device offset
Ksend = 0.03;
%%% Rotation %%%%
Je = (pi*(ma/2)^3*(mi/2)^3)/((ma/2)^2+(mi/2)^2); % Torsion ...
    constant rectangle
Rote = (Mx*ls)/(G*Je)*(180/pi); % angular ...
    rotation due to torque
kr = mean(Mx./Rote);        % torsional ...
    spring constant
Rotea = Rote - Rote*Ksenr;
%%
figure
plot(Fs,Rote(1,:),Fs,Rote(2,:),Fs,Rote(3,:),Fs,Rote(4,:))
legend('L-{\whisker} = 1mm','L-{\whisker} = 10mm','L-{\whisker} = ...
    20mm','L-{\whisker} = 30mm')
title('Force vs Rotation')
xlabel('Force (N)')
ylabel('Angle (Deg)')
%%

% stress and stress data
shear_stress = (2.*Mx)/(pi*ma/2*(mi/2)^2) ; % flexural ...
    stress due to torque
% shear_strain = ma*Rotea/ls; % Strain ...
    (r*theta)/ls
shear_strain = shear_stress./G;
%%
figure
subplot(2,2,1)
plot(shear_strain(1,:),shear_stress(1,:))
% line([elong_break elong_break],[0 ...
    max(shear_stress(1,:))],'color','r');
% legend('Stress Strain Curve','% Elongation at break')
title('L-{\whisker}= 1mm')

```

```

xlabel('Shear strain')
ylabel('Shear stress (MPa)')
subplot(2,2,2)
plot(shear_strain(2,:),shear_stress(2,:))
line([elong_break elong_break],[0 ...
    max(shear_stress(2,:))],'color','r');
legend('Stress Strain Curve','% Elongation at break')
title('L.{whisker}= 10mm')
xlabel('Shear strain')
ylabel('Shear stress (MPa)')
subplot(2,2,3)
plot(shear_strain(3,:),shear_stress(3,:))
line([elong_break elong_break],[0 ...
    max(shear_stress(3,:))],'color','r');
legend('Stress Strain Curve','% Elongation at break')
title('L.{whisker}= 20mm')
xlabel('Shear strain')
ylabel('Shear stress (MPa)')
subplot(2,2,4)
plot(shear_strain(4,:),shear_stress(4,:))
line([elong_break elong_break],[0 ...
    max(shear_stress(4,:))],'color','r');
legend('Stress Strain Curve','% Elongation at break')
title('L.{whisker}= 30mm')
xlabel('Shear strain')
ylabel('Shear stress (MPa)')
annotation('textbox', [0 0.9 1 0.1], ...
    'String', 'Shear stress vs Shear strain', ...
    'EdgeColor', 'none', ...
    'HorizontalAlignment', 'center')
%%
%%% Translation %%%
Ie = pi*(ma*(mi/2)^3)/4; % Area moment of inertia
%Defe = ((Fs*(2*ls)^3)/(48*E*Ie)); % Maximum deflection at ...
    support rectangular cantilever
Defe = (Fs*ls.^3)/(6*E*Ie);
% Defea = (Fs*ls.^3)/(192*E*Ie) - Ksend*Defe; % ...
    Displacement of whisker base
kt = mean(Fs./Defe);
figure
plot(Fs,Defe)
title('Deflection vs Force')
xlabel('Force (N)')
ylabel('Displacement (mm)')

%%
% circumferential stress
% Mb = Fs*ls; % Bending moment
% R = (ma/2)^2/(mi/2); % Radius of curvature
% c = mi/2; % Distance from center to ...
    extreme fiber on concave side
% ec = 1/2*(R/c-sqrt((R/c)^2-1)); % Ratio for stress calc
% alph = 1/(4*ec)*(1-ec)/(R/c-1); % Ratio for strss calc
% cir_stress = alph*Mb*c/Ie;

dls =sqrt(ls.^2 + Defe.^2)-ls;
cir_strain = dls./ls;
cir_stress = E.*cir_strain;
figure
plot(cir_strain,cir_stress)
title('Shear strain vs Shear stress due to Deflection')
xlabel('Shear strain')

```

```

ylabel('Shear stress (MPa)')

%%%%%%%%%%%%%%%%%%%%%%%%%%%%%%%%%%%%%%%%%%%%%%%%%%%%%%%%%%%%%%%%%%%%%%%%
%%%%%%%%%% Model Validation ...
%%%%%%%%%%%%%%%%%%%%%%%%%%%%%%%%%%%%%%%%%%%%%%%%%%%%%%%%%%%%%%%%%%%%%%%%
clc
close all;
clear all
E = 3.5e3; % Young's Modulus MPa
G = 2.4e3; % Shear Modulus MPa
lw = [1; 10 ;20 ;30]; % Whisker length
ls = 10; % Distance from support base to outer ...
square
mi = 1.6; % minor axis
ma = 3.2; % major axis
w = [0 9.32 119.42 119.13 121.40 119.54 122.07]./1000; % weights used
wr = size(w,2); % summation of weights
for i=1:size(w,2)
    if i == 1
        wr(i) = 0;
    else
        wr(i) = wr(i-1)+w(i);
    end
end
set(groot, 'defaultAxesLineStyleOrder', {'-'})
F = (9.81.*wr)*(1-2.7012e-2); % Force due to wieghts used ...
minusmeasurement offset
Mx = lw*F;
%% Import
file = 'whisker_structure_data.xls';
addpath('/media/john/DCDAE004DADFD8BA/Bachelor Project/Report/Matlab')
M = readtable(file);
time = transpose(table2array(M(:,1)));
% L0 = transpose(table2array(M(:,2)));
% L1 = transpose(table2array(M(:,3)));
% L2 = transpose(table2array(M(:,4)));
L3 = transpose(table2array(M(:,5)));
% LH = transpose(table2array(M(:,6)));
T = transpose(table2array(M(:,7)));
% TH = transpose(table2array(M(:,8)));
%% Rotation data and analysis
% expected behaviour rotation
Je = (pi*(ma/2)^3*(mi/2)^3)/((ma/2)^2+(mi/2)^2); % Torsion ...
constant rectangle
Rote = ((Mx*ls)/(G*Je))*(180/pi); % Expected ...
twist angle due to torque
% rotation twist caused by force
l0 = [0 0 0.3736 0.8281 1.301 1.773 2.198 1.978 ...
1.586 1.15 0.644 0.1406 0.0855]; %
l1 = [0 1.892 4.057 6.176 8.611 7.28 5.217 3.128 0.5867 0.2865];
l2 = [0 0.1711 3.752 7.427 11.75 9.128 5.433 1.405 0.9732];
l3 = [0 0.3942 5.599 11.21 6.889 1.377 0.6982];

l0u = l0(1,1:7);
l0d = fliplr(l0(1,7:13));
l1u = l1(1,1:5);
l1d = fliplr(l1(1,5:9));
l2u = l2(1,1:5);
l2d = fliplr(l2(1,5:9));
l3u = l3(1,1:4);

```

```

l3d = fliplr(l3(1,4:7));
%% Hysteresis plots Rotation
figure
subplot(2,2,1)
plot(F,l0u,F,l0d)
legend('Increasing load','Decreasing load')
xlabel('Force (N)')
ylabel('Rotation (Deg)')
title('L_{whisker}= 1 mm')
subplot(2,2,2)
plot(F(1,2:6),l1u,F(1,2:6),l1d)
legend('Increasing load','Decreasing load')
xlabel('Force (N)')
ylabel('Rotation (Deg)')
title('L_{whisker}=10 mm')
subplot(2,2,3)
plot(F(1,1:5),l2u,F(1,1:5),l2d)
legend('Increasing load','Decreasing load')
xlabel('Force (N)')
ylabel('Rotation (Deg)')
title('L_{whisker}=20 mm')
subplot(2,2,4)
plot(F(1,1:4),l3u,F(1,1:4),l3d)
legend('Increasing load','Decreasing load')
xlabel('Force (N)')
ylabel('Rotation (Deg)')
title('L_{whisker}=30 mm')
annotation('textbox', [0 0.9 1 0.1], ...
    'String', 'Hysteresis Plots Rotation', ...
    'EdgeColor', 'none', ...
    'HorizontalAlignment', 'center')
%% loading plots Rotation
figure
subplot(2,2,1)
plot(F,l0u,'o',F,Rote(1,:))
legend('Measurement','Expected')
xlabel('Force (N)')
ylabel('Rotation (Deg)')
title('Loading L_{whisker}=1 mm')
subplot(2,2,2)
plot(F(1,2:6),l1u,'o',F(1,2:6),Rote(2,2:6))
legend('Measurement','Expected')
xlabel('Force (N)')
ylabel('Rotation (Deg)')
title('Loading L_{whisker}=10 mm')
subplot(2,2,3)
plot(F(1,1:5),l2u,'o',F(1,1:5),Rote(3,1:5))
legend('Measurement','Expected')
xlabel('Force (N)')
ylabel('Rotation (Deg)')
title('Loading L_{whisker}=20 mm')
subplot(2,2,4)
plot(F(1,1:4),l3u,'o',F(1,1:4),Rote(4,1:4))
legend('Measurement','Expected')
xlabel('Force (N)')
ylabel('Rotation (Deg)')
title('Loading L_{whisker}=30 mm')
annotation('textbox', [0 0.9 1 0.1], ...
    'String', 'Expected vs Measured Rotation', ...
    'EdgeColor', 'none', ...
    'HorizontalAlignment', 'center')

```

```

%% Spring constants rotation
% Rotational constant
% Expected
kre = mean(mean(Mx(:,2:end)'./Rote(:,2:end)'));
krm0 = mean((Mx(1,3:7))./l0u(3:7));
krm1 = mean((Mx(2,3:6))./l1u(2:5));
krm2 = mean((Mx(3,2:5))./l2u(2:5));
krm3 = mean((Mx(4,2:4))./l3u(2:4));
krm = [krm0 krm1 krm2 krm3];
kkr = krm/kre;
figure
plot(lw,kkr,'o');
xlabel('Whisker length (mm)')
ylabel('k_{measured}/k_{expected} ')
% line([0 max(lw)], [kre kre], 'color', 'r')
title('Torsional Spring Constant')
% legend('Measured', 'Expected')
%% Creep Rotation
cr = (L3(1,544:789) - L3(1,544));
tr = (time(1,544:789) - time(1,544))./1000;
figure
plot(tr,cr)
xlabel('Time (s)')
ylabel('Rotation (deg)')
title('Rotation Creep')
%% Displacement data and analysis
t0 = [0 0.0181 0.0539 0.0897 0.1237 0.1777 0.1653 0.1386 0.1088 ...
      0.0754 0.0383];
tu = t0(1,1:6);
td = fliplr(t0(1,6:11));

% expected behaviour displacement
Ie = pi*(ma*(mi/2)^3)/4; % Area moment of inertia
Def = (F(1,2:end)*ls.^3)./(6*E*Ie); % expected deflection
%% displacement comparison
figure
plot(F(1,2:end),tu,'o',F(1,2:end),Def);
legend('Measured','Expected')
xlabel('Force (N)')
ylabel('Deflection (mm)')
title('Expected vs Measured displacement')
%% Hysteresis
figure
plot(F(1,2:end),tu,F(1,2:end),td);
legend('Increase load','Decrease load')
xlabel('Force (N)')
ylabel('Deflection (mm)')
title('Displacement Hysteresis')
%% spring constant Displacement
kte = mean(F(1,2:end)./Def);
ktm = F(1,3:end)./tu(1,2:6);
kkt = ktm./kte;
figure
plot(F(1,3:end),kkt,'o')
% line([min(F(1,3:end)) max(F(1,3:end))], [kte kte], 'color', 'r');
% legend('Measured', 'Expected')
xlabel('Force(N)')
ylabel('k_{measured}/k_{expected}')
title('Displacement Spring Constant')
%% Creep Displacement
ct = (T(1,1085:1315) - T(1,1085));
tt = (time(1,1085:1315) - time(1,1085))./1000;

```

```
figure
plot(tt,ct)
xlabel('Time (s)')
ylabel('Displacement (mm)')
title('Displacement Creep')
```

F Openscad Code

```
$fn = 30;

// Outer support base values
w_outer = 4; // outer square width
t_outer = 4 ; // outer square height

// Flex beam (spring) values
s_major = 1.6; // spring half major axis
s_minor = 0.8; // spring half minor axis default ...
           = 1.3
s_length = 8; // spring length

// Whisker support base values
w_support= 5; // whisker base width
t_support = t_outer; // whisker base thickness

// Extensions from base to dielectric
t_extension = 2; // base extension thickness
l_extension =s_length/2 +1; // length extension
w_extension = w_support/2; // extension width

// Dielectric material values
distance = 0; // distance from trace to dielectric
r_dielectric = 2.5; // dimension dielectric
t_dielectric = 2; // thickness dielectric

//Whisker dimensions
l_whisker = 50; // whisker length
r_whisker = 1; // whisker radius
l_connector = 4;

module ellipse(h,w ){
    scale([w,h])circle(r = 1);
}

module support( h,w,l){
    rotate([90,0,0]){
        linear_extrude(s_length+0.05)
            ellipse(h,w);
    }
}

module outer_square(s_length,w_support,w_outer){
    var = 2*s_length+(w_support);
    difference(){
        square((var + 2*w_outer), center = true);
        square(var, center = true );
    }
}

module whisker_base(){
    union(){
        // Support base
        translate([0,0,-t_support])
            linear_extrude(t_support)
                square(w_support,center = true);
    }
}
```

```

// extension 1 for dil.extensionelectric for cap
translate([(l.extension/2+w.support/2),0,-t.extension])
  linear_extrude(t.extension)
    scale([1.05,0.5,1])square(l.extension,center = true);
translate([(w.support/2+l.extension),0,-(t.extension+t.dielectric-0.1)])
  linear_extrude(t.dielectric)
    square([2*r.dielectric,6*r.dielectric], center = true);

// extension 2 for dil.extensionelectric for cap
translate([-l.extension/2+w.support/2),0,-t.extension])
  linear_extrude(t.extension)
    scale([1.05,0.5,1])square(l.extension,center = true);
translate([-w.support/2+l.extension),0,-(t.extension+t.dielectric-0.1)])
  linear_extrude(t.dielectric)
    square([2*r.dielectric,6*r.dielectric], center = true);
}
}
module base(){
  union(){
    rotate([180,0,0]){
      linear_extrude(t.outer){
        outer.square(s.length,w.support,w.outer);
      }
    }
    translate([0,(-w.support/2),-s.major])
      support(s.major,s.minor,s.length);
    translate([0,(s.length+w.support/2),-s.major])
      support(s.major,s.minor,s.length);
  }
}
module whisker(){
  translate([0,0,-0,-5])
    linear_extrude(l.whisker)
      circle(r.whisker,center = true);
}

module connector(){
  rotate([180,0,0]){
    difference(){
      union(){
        difference(){
          union(){
            linear_extrude(l.connector+0.05)
              circle(w.outer/2 , center = true);
            translate([0,0,l.connector])
              linear_extrude(2)
                circle((w.outer/2)+0.2,center = true);
          }
        }
        translate([0,(t.outer/2)+1,4])
          cube([w.outer,2,8], center = true);
        translate([0,-(t.outer/2)-1,4])
          cube([w.outer,2,8], center = true);
      }
    }
    translate([0,0,5])
      cube([2,t.outer+1,4], center = true);
  }
}
}
}

```

```

module connector_pattern(){
  translate([0,(w_support/2 + s_length + ...
    w_outer/2),-(t_support-0.05)])
  connector();
  translate([0,-(w_support/2 + s_length + ...
    w_outer/2),-(t_support-0.05)])
  connector();
  translate([(w_support/2 + s_length + ...
    w_outer/2),0,-(t_support-0.05)])
  connector();
  translate([-w_support/2 + s_length + ...
    w_outer/2),0,-(t_support-0.05)])
  connector();
}

module base_modl_extension(){
  union(){
    difference(){
      whisker_base();
      translate([0,0,-5])
      whisker();
    }

    base();
    connector_pattern();
  }
}

module full_model(){
  whisker_base();
  whisker();
  base();
  connector_pattern();
}
//translate([0,0,-2])
full_model();
//base_modl_extension();

```